

1 *The h term in Equation (25a) and Equation (25b) defines vertical distance from a reference*
 2 *point. In the CRA-2004 PA, this reference point is taken to be the center of MB 139 at the*
 3 *location of the shaft (i.e., $(x_{ref}, y_{ref}) = (23664.9 \text{ m}, 378.685 \text{ m})$, which is the center of cell*
 4 *1266 in Figure PA-10). Specifically, h is defined by*

$$5 \quad h(x, y) = (x - x_{ref}) \sin \theta + (y - y_{ref}) \cos \theta, \quad (27)$$

6 *where θ is the inclination of the formation in which the point (x, y) is located. In the CRA-*
 7 *2004 PA, the Salado Formation is modeled as having an inclination of 1° from north to south,*
 8 *and all other formations are modeled as being horizontal. Thus, $\theta = 1^\circ$ for points within the*
 9 *Salado, and $\theta = 0^\circ$ otherwise. Treating the Salado as an inclined formation and treating the*
 10 *Castile Formation, Castile brine reservoir, Rustler Formation, and overlying units as*
 11 *horizontal creates discontinuities in the grid at the lower and upper boundaries of the Salado.*
 12 *However, this treatment does not create a computational problem, since the Salado is isolated*
 13 *from vertical flow; its upper boundary adjoins the impermeable Los Medaños Member*
 14 *(formerly referred to as the Unnamed Member) at the base of the Rustler Formation, and its*
 15 *lower boundary adjoins the impermeable Castile Formation.*

16 *In the solution of Equation (25), S_b and S_g are functions of location and time. Thus, p_C , k_{rb}*
 17 *and k_{rg} are functions of the form $p_C(x, y, t)$, $k_{rb}(x, y, t)$, and $k_{rg}(x, y, t)$. In the*
 18 *computational implementation of the solution of the preceding equations, flow of phase l out*
 19 *of a computational cell (Figure PA-10) cannot occur when $S_l(x, y, t) \leq S_{lr}(x, y, t)$, where S_{lr}*
 20 *denotes the residual saturation for phase l . The values used for S_{lr} , $l = b, g$ are summarized*
 21 *in Table PA-2.*

22 *Values for ϕ_0 and β_f (Equation (25g)) are also given in Table PA-2. Initial porosity ϕ_0 for the*
 23 *DRZ is a function of the uncertain parameter for initial halite porosity ϕ_{0H} (HALPOR; see*
 24 *Table PA-17) and is given by Martell (1996a, Chapter 4; Bean et al. 1996)*

$$25 \quad \phi_0 = \phi_{0H} + 0.0029. \quad (28)$$

26 *This representation is used because the DRZ and halite porosities are correlated, with the*
 27 *high, low, and median porosity values for the DRZ being 0.0029 higher than the*
 28 *corresponding undisturbed halite values. Initial porosity ϕ_0 of the Castile brine reservoir is*
 29 *correlated to the uncertain sampled parameter for bulk compressibility (BPCOMP; see Table*
 30 *PA-17), according to the following relationship:*

$$31 \quad \phi_0 = \frac{BPCOMP}{1.0823 \times 10^{-10}}, \quad (29)$$

32 *where 1.0860×10^{-10} is a scaling constant that ensures that the productivity ratio, PR ,*
 33 *remains constant at $2.0 \times 10^{-3} \text{ m}^3/\text{Pa}$. The productivity ratio PR is computed by*

Table PA-2. Parameter Values Used in Representation of Two Phase Flow

Region	Material	Material Description	Brooks-Corey Pore Distribution λ	Threshold Pressure Linear Parameter a	Threshold Pressure Exponential Parameter η	Residual Brine Saturation S_{br}	Residual Gas Saturation S_{gr}	Porosity ϕ_0	Pore Compressibility β_f	Intrinsic Permeability k, m^2
Salado	S_HALITE	Undisturbed halite	0.7	0.56	-0.346	0.3	0.2	HALPOR1	f(HALCOMP1)3	10x, x = HALPRM1
Upper DRZ	DRZ_0	Disturbed rock zone, -5 to 0 years	0.7	0.0	0.0	0.0	0.0	f(HALPOR1)2	f(HALCOMP1)3	9.999999 x 10-18
	DRZ_1	Disturbed rock zone, 0 to 10,000 years	0.7	0.0	0.0	0.0	0.0	f(HALPOR1)2	f(HALCOMP1)3	10x, x = DRZPRM1
Lower DRZ	DRZ_0	Disturbed rock zone, -5 to 0 years	0.7	0.0	0.0	0.0	0.0	f(HALPOR1)2	f(HALCOMP1)3	9.999999 x 10-18
	DRZ_1	Disturbed rock zone, 0 to 10,000 years	0.7	0.0	0.0	0.0	0.0	f(HALPOR1)2	f(HALCOMP1)3	10x, x = DRZPRM1
MB 138	S_MB138	Anhydrite marker bed in Salado Formation	ANHBCEXP1	0.26	-0.348	ANRBSAT1	ANRGSSAT1	0.011	f(ANHCOMP1)3	10x, x = ANHPRM1
Anhydrite AB	S_ANH_AB	Anhydrite layers a and b in Salado Formation	ANHBCEXP1	0.26	-0.348	ANRBSAT1	ANRGSSAT1	0.011	f(ANHCOMP1)3	10x, x = ANHPRM1
MB 139	S_MB139	Anhydrite marker bed in Salado Formation	ANHBCEXP1	0.26	-0.348	ANRBSAT1	ANRGSSAT1	0.011	f(ANHCOMP1)3	10x, x = ANHPRM1
Waste Panel	CAVITY_1	Single waste panel, -5 to 0 years	0.7	0.0	0.0	0.0	0.0	1.0	0.0	1.0 x 10-10
	WAS_AREA	Single waste panel, 0 to 10,000 years	2.89	0.0	0.0	WRBRNSAT1	WRGSSAT1	0.8485	0.0	2.4 x 10-13
South RoR	CAVITY_2	Rest of repository, -5 to 0 years	0.7	0.0	0.0	0.0	0.0	1.0	0.0	1.0 x 10-10
	REPOSIT	Rest of repository, 0 to 10,000 years	2.89	0.0	0.0	WRBRNSAT1	WRGSSAT1	0.848 5	0.0	2.4 x 10-13
North RoR	CAVITY_2	Rest of repository, -5 to 0 years	0.7	0.0	0.0	0.0	0.0	1.0	0.0	1.0 x 10-10
	REPOSIT	Rest of repository, 0 to 10,000 years	2.89	0.0	0.0	WRBRNSAT1	WRGSSAT1	0.848 5	0.0	2.4 x 10-13
Ops	CAVITY_3	Operations area, -5 to 0 years	0.7	0.0	0.0	0.0	0.0	1.0	0.0	1.0 x 10-10
	OPS_AREA	Operations area, 0 to 10,000 years	0.7	0.0	0.0	0.0	0.0	0.18	0.0	1.0 x 10-11

Table PA-2. Parameter Values Used in Representation of Two Phase Flow — Continued

Region	Material	Material Description	Brooks-Corey Pore Distribution λ	Threshold Pressure Linear Parameter a	Threshold Pressure Exponential Parameter η	Residual Brine Saturation S_{br}	Residual Gas Saturation S_{gr}	Porosity ϕ_0	Pore Compressibility β_f	Intrinsic Permeability k, m^2
Exp	CAVITY_3	Experimental area, -5 to 0 years	0.7	0.0	0.0	0.0	0.0	1.0	0.0	1.0×10^{-10}
	EXP_AREA	Experimental area, 0 to 10,000 years	0.7	0.0	0.0	0.0	0.0	0.18	0.0	1.0×10^{-11}
Castile	IMPERM_Z	Castile Formation	0.7	0.0	0.0	0.0	0.0	0.005	0.0	9.999999×10^{-36}
Castile Brine Reservoir	CASTILER	Brine Reservoir in Castile Formation	0.7	0.56	-0.346	0.2	0.2	$f(BPCOMP\ 1)^4$	$f(BPCOMP\ 1)^3$	$10x, x = BPPRMI$
Culebra	CULEBRA	Culebra Member of Rustler Formation	0.6436	0.26	-0.348	0.08363	0.07711	0.151	6.622517×10^{-10}	2.098938×10^{-14}
Magenta	MAGENTA	Magenta Member of Rustler Formation	0.6436	0.26	-0.348	0.08363	0.07711	0.138	1.915942×10^{-9}	6.309576×10^{-16}
Dewey Lake	DEWYLAKE	Dewey Lake Redbeds	0.6436	0.0	0.0	0.08363	0.07711	0.143	6.993007×10^{-8}	5.011881×10^{-17}
Santa Rosa	SANTAROS	Santa Rosa Formation	0.6436	0.0	0.0	0.08363	0.07711	0.175	5.714286×10^{-8}	1.0×10^{-10}
Los Medanos	UNNAMED	Los Medaños Member of Rustler Formation	0.7	0.0	0.0	0.2	0.2	0.181	0.0	9.999999×10^{-36}
Tamarisk	TAMARISK	Tamarisk Member of Rustler Formation	0.7	0.0	0.0	0.2	0.2	0.064	0.0	9.999999×10^{-36}
49er	FORTYNIN	Fortyniner Member of Rustler Formation	0.7	0.0	0.0	0.2	0.2	0.082	0.0	9.999999×10^{-36}
DRZ_PCS	DRZ_0	Disturbed rock zone, -5 to 0 years	0.7	0.0	0.0	0.0	0.0	$f(HALPOR1)^2$	$f(HALCOMP1)^3$	9.999999×10^{-18}
DRZ_PCS	DRZ_PCS	DRZ above the panel closures, 0 to 10,000 years	0.7	0.0	0.0	0.0	0.0	$f(HALPOR1)^2$	$f(HALCOMPa)^c$	$10x, x = DRZPCPRMI$
CONC_PCS	CAVITY_4	Concrete portion of panel closures, -5 to 0 years	0.7	0.0	0.0	0.0	0.0	1.0	0.0	1.0×10^{-10}
	CONC_PCS	Concrete portion of panel closures, 0 to 10,000 years	0.9193	0.0	0.0	CONBRSATI	CONGSSATI	0.005	1.2×10^{-9}	$10x, x = CONPRMI$
DRF_PCS	CAVITY_4	Drift adjacent to panel closures, -5 to 0 years	0.7	0.0	0.0	0.0	0.0	1.0	0.0	1.0×10^{-10}

Table PA-2. Parameter Values Used in Representation of Two Phase Flow — Continued

Region	Material	Material Description	Brooks-Corey Pore Distribution λ	Threshold Pressure Linear Parameter a	Threshold Pressure Exponential Parameter η	Residual Brine Saturation S_{br}	Residual Gas Saturation S_{gr}	Porosity ϕ_0	Pore Compressibility β_f	Intrinsic Permeability k, m^2
	<i>DRF_PCS</i>	<i>Drift adjacent to panel closures, 0 to 10,000 years</i>	2.89	0.0	0.0	<i>WRBRNSATI</i>	<i>WRGSSATI</i>	0.848	0.0	2.4×10^{-13}
<i>CONC_MON</i>	<i>CAVITY_4</i>	<i>Concrete monolith portion of shaft seals, -5 to 0 years</i>	0.7	0.0	0.0	0.0	0.0	1.0	0.0	1.0×10^{-10}
	<i>CONC_MON</i>	<i>Concrete monolith portion of shaft seals, 0 to 10,000 years</i>	0.94	0.0	0.0	<i>SHURBRNI</i>	<i>SHURGASI</i>	0.05	1.2×10^{-9}	1.0×10^{-14}
<i>Upper Shaft</i>	<i>CAVITY_4</i>	<i>Upper portion of shaft seals, -5 to 0 years</i>	0.7	0.0	0.0	0.0	0.0	1.0	0.0	1.0×10^{-10}
	<i>SHFTU</i>	<i>Upper portion of shaft seals, 0 to 10,000 years</i>	0.9193	0.0	0.0	<i>SHURBRNI</i>	<i>SHURGASI</i>	0.005	2.05×10^{-8}	$10x, x = SHUPRM1$
<i>Lower Shaft</i>	<i>CAVITY_4</i>	<i>Lower portion of shaft seals, -5 to 0 years</i>	0.7	0.0	0.0	0.0	0.0	1.0	0.0	1.0×10^{-10}
	<i>SHFTL_T1</i>	<i>Lower portion of shaft seals, 0 - 200 years</i>	0.9193	0.0	0.0	<i>SHURBRNI</i>	<i>SHURGASI</i>	0.005	4.28×10^{-9}	$10x, x = SHLPRM11$
	<i>SHFTL_T2</i>	<i>Lower portion of shaft seals, 200 - 10,000 years</i>	0.9193	0.0	0.0	<i>SHURBRNI</i>	<i>SHURGASI</i>	0.005	4.28×10^{-9}	$10x, x = SHLPRM21$
<i>Borehole plugs</i>	<i>CONC_PLG</i>	<i>Concrete borehole plug, before plug degradation</i>	0.94	0.0	0.0	0.0	0.0	0.32	0.0	$10x, x = PLGPRM1$
	<i>BH_SAND</i>	<i>Borehole after plug degradation, 200 years after intrusion</i>	0.94	0.0	0.0	0.0	0.0	0.32	0.0	$10x, x = BHPRM1$
<i>Upper Borehole</i>	<i>BH_OPEN</i>	<i>Borehole above repository before plug degradation</i>	0.7	0.0	0.0	0.0	0.0	0.32	0.0	1.0×10^{-9}
	<i>BH_SAND</i>	<i>Borehole after plug degradation, 200 years after intrusion</i>	0.94	0.0	0.0	0.0	0.0	0.32	0.0	$10x, x = BHPRM1$
<i>Lower Borehole</i>	<i>BH_OPEN</i>	<i>Borehole below repository before creep closure</i>	0.7	0.0	0.0	0.0	0.0	0.32	0.0	1.0×10^{-9}

Table PA-2. Parameter Values Used in Representation of Two Phase Flow — Continued

<i>Region</i>	<i>Material</i>	<i>Material Description</i>	<i>Brooks-Corey Pore Distribution λ</i>	<i>Threshold Pressure Linear Parameter a</i>	<i>Threshold Pressure Exponential Parameter η</i>	<i>Residual Brine Saturation S_{br}</i>	<i>Residual Gas Saturation S_{gr}</i>	<i>Porosity ϕ_0</i>	<i>Pore Compressibility β_f</i>	<i>Intrinsic Permeability k, m^2</i>
	<i>BH_CREEP</i>	<i>Borehole below repository after creep closure, 1,000 years after intrusion</i>	<i>0.94</i>	<i>0.0</i>	<i>0.0</i>	<i>0.0</i>	<i>0.0</i>	<i>0.32</i>	<i>0.0</i>	<i>10x/10, x = BHPRMI</i>

¹ *Uncertain variable, see Table PA-17.*

² *See Equation (28).*

³ *See Equation (31); ϕ_0 can also be defined by an uncertain variable.*

⁴ *See Equation (29).*

⁵ *Initial value of porosity ϕ_0 ; porosity changes dynamically to account for creep closure (see Section PA-4.2.3).*

1
$$PR = V \frac{BPCOMP}{\phi_0}, \quad (30)$$

2 *where V is the volume of the grid block representing the Castile brine reservoir in Figure*
 3 *PA-8. The effect of this relationship is that the initial porosity of the brine reservoir ranges*
 4 *from 0.1842 to 0.9208. This range of porosity is not meant to represent an actual reservoir,*
 5 *but rather allows a reservoir to supply a volume of brine to the repository in the event of an E1*
 6 *intrusion consistent with observed brine flows in the Delaware Basin.*

7 *The compressibility β_f in Equation (25f) and Table PA-2 is pore compressibility.*
 8 *Compressibility is treated as uncertain for Salado anhydrite, Salado halite, and regions of*
 9 *pressurized brine in the Castile Formation. However, the sampled value for each of these*
 10 *variables corresponds to bulk compressibility rather than to the pore compressibility actually*
 11 *used in the calculation. The conversion from bulk compressibility β_{fB} to pore compressibility*
 12 *β_f is approximated by*

13
$$\beta_f = \beta_{fB} / \phi_0, \quad (31)$$

14 *where ϕ_0 is the initial porosity in the region under consideration.*

15 *The primary model used in the CRA-2004 PA for capillary pressure p_C and relative*
 16 *permeability $k_{r,l}$ is a modification of the Brooks-Corey model (Brooks and Corey 1964). In this*
 17 *model, p_C , k_{rb} and k_{rg} are defined by*

18
$$p_C = p_t(k) / S_{e2}^{1/\lambda} \quad (32a)$$

19
$$k_{rb} = S_{e1}^{(2+3\lambda)/\lambda} \quad (32b)$$

20
$$k_{rg} = (1 - S_{e2})^2 \left(1 - S_{e2}^{(2+\lambda)/\lambda} \right), \quad (32c)$$

21 *where*

22 $\lambda =$ *pore distribution parameter (dimensionless)*

23 $p_t(k) =$ *capillary threshold pressure (Pa) as a function of intrinsic*
 24 *permeability k (Webb 1992)*
 25 $= ak^\eta \quad (33)$

26 $S_{e1} =$ *effective brine saturation (dimensionless) without correction for*
 27 *residual gas saturation*
 28 $= (S_b - S_{br}) / (1 - S_{br}) \quad (34)$

$$\begin{aligned}
 S_{e2} &= \text{effective brine saturation (dimensionless) with correction for} \\
 &\quad \text{residual gas saturation} \\
 &= (S_b - S_{br}) / (1 - S_{gr} - S_{br}) .
 \end{aligned}
 \tag{35}$$

The values used for λ , a , η , S_{br} , S_{gr} , and k are summarized in Table PA-2. The statement that the Brooks-Corey model is in use means that p_C , k_{rb} , and k_{rg} are defined by Equation (32). The Brooks-Corey model is used for all materials with the two exceptions, as identified in Table PA-3. In the anhydrite MBs, either the Brooks-Corey model or the van Genuchten-Parker model is used as determined by the subjectively uncertain parameter ANHBCVGP (see Table PA-17). A linear model is used in the representation of two-phase flow in an open borehole (i.e., for the first 200 years after a drilling intrusion for boreholes with two-plug or three-plug configurations (Section 6.4.7.2)). Each of these alternatives to the Brooks-Corey model is now discussed.

Table PA-3. Models for Relative Permeability and Capillary Pressure for Two-Phase Flow

Material	Relative Permeability ¹	Capillary Pressure ²	Material	Relative Permeability ¹	Capillary Pressure ²
S_HALITE	4	2	WAS_AREA	4	1
DRZ_0	4	1	DRZ_1	4	1
S_MB139	ANHBCVGP ³	2	DRZ_PCS	4	1
S_ANH_AB	ANHBCVGP ³	2	CONC_PCS	4	1
S_MB138	ANHBCVGP ³	2	UNNAMED	4	1
CAVITY_1	4	1	TAMARISK	4	1
CAVITY_2	4	1	FORTYNIN	4	1
CAVITY_3	4	1	DRF_PCS	4	1
CAVITY_4	4	1	REPOSIT	4	1
IMPERM_Z	4	1	CONC_MON	4	1
CASTILER	4	2	SHFTU	4	1
OPS_AREA	4	1	SHFTL_T1	4	1
EXP_AREA	4	1	SHFTL_T2	4	1
CULEBRA	4	2	CONC_PLG	4	1
MAGENTA	4	2	BH_OPEN	5	1
DEWYLAKE	4	1	BH_SAND	4	1
SANTAROS	4	1	BH_CREEP	4	1

¹ Relative permeability model, where 4 ~ Brooks-Corey model (Equation (32)), 5 ~ linear model (Equation (37)), and ANHBCVGP ~ use of Brooks-Corey or van Genuchten-Parker model treated as a subjective uncertainty.

² Capillary pressure model, where 1 ~ $p_C = 0$ Pa, 2 ~ p_C bounded above by 1×10^8 Pa as S_b approaches S_{br}

³ See ANHBCVGP in Table PA-17.

1 *In the van Genuchten-Parker model, p_C , k_{rb} , and k_{rg} are defined by (van Genuchten 1978):*

2
$$p_C = p_{VGP} \left(S_{e2}^{-1/m} - 1 \right)^{1-m} \quad (36a)$$

3
$$k_{rb} = S_{e1}^{1/2} \left[1 - \left(1 - S_{e1}^{1/m} \right)^m \right]^2 \quad (36b)$$

4
$$k_{rg} = \left(1 - S_{e2} \right)^{1/2} \left(1 - S_{e2}^{1/m} \right)^{2m}, \quad (36c)$$

5 *where $m = \lambda / (1 + \lambda)$ and the capillary pressure parameter p_{VGP} is determined by requiring*
 6 *that the capillary pressures defined in Equation (32a) and Equation (36a) are equal at an*
 7 *effective brine saturation of $S_{e2} = 0.5$ (Webb 1992). The van Genuchten-Parker model is*
 8 *only used for the anhydrite MBs in the Salado and uses the same values for λ , S_{br} , and S_{gr} as*
 9 *the Brooks-Corey model (Table PA-2).*

10 *In the linear model, p_C , k_{rb} , and k_{rg} are defined by:*

11
$$p_C = 0, k_{rb} = S_{e1}, k_{rg} = 1 - S_{e1}. \quad (37)$$

12 *Capillary pressure p_C for both the van Genuchten-Parker and Brooks-Corey models becomes*
 13 *unbounded as brine saturation S_b approaches the residual brine saturation, S_{br} . To avoid*
 14 *unbounded values, p_C is capped at 1×10^8 Pa in selected regions (Table PA-3).*

15 *The saturation and capillary pressure constraints (i.e., Equation (25c) and Equation (25d))*
 16 *permit a reduction of the number of equations to be solved from four to two. In particular, the*
 17 *constraint equations are used to reformulate Equation (25a) and Equation (25b) so that the*
 18 *unknown functions are gas saturation S_g and brine pressure p_b . Specifically, the saturation*
 19 *constraint in Equation (25c) allows S_b to be expressed as*

20
$$S_b = 1 - S_g, \quad (38)$$

21 *and thus allows S_{e1} and S_{e2} in Equation (34) and Equation (35) to be reformulated as*

22
$$S_{e1} = \left(1 - S_g - S_{br} \right) / \left(1 - S_{br} \right) \quad (39)$$

23
$$S_{e2} = \left(1 - S_g - S_{br} \right) / \left(1 - S_{gr} - S_{br} \right). \quad (40)$$

24 *Further, the capillary pressure constraint in Equation (25d) allows p_g to be expressed as*

25
$$p_g = p_b + p_C$$

$$1 \quad = p_b + p_t(k) / S_e^{1/2} \quad \text{for Brooks-Corey model, Equation (32a)} \quad (41a)$$

$$2 \quad = p_b + p_{VGP} \left(S_e^{-1/m} - 1 \right)^{1-m} \quad (41b)$$

3 *for van Genuchten-Parker model, Equation (36a)*

$$4 \quad = p_b \quad \text{for linear model, Equation (37).} \quad (41c)$$

5 *The equalities in Equation (39), Equation (40), and Equation (41) allow the transformation of*
 6 *Equation (25a) and Equation (25b) into two equations whose unknown functions are S_g and*
 7 *p_b , which are the equations that are actually solved in BRAGFLO:*

$$8 \quad \nabla \cdot \left[\frac{\alpha \rho_g K_g k_{rg}}{\mu_g} (\nabla p_g + \rho_g g \nabla h) \right] + \alpha q_{wg} + \alpha q_{rg} = \alpha \frac{\partial (\phi \rho_g S_g)}{\partial t} \quad (42a)$$

$$9 \quad \nabla \cdot \left[\frac{\alpha \rho_b K_b k_{rb}}{\mu_b} (\nabla p_b + \rho_b g \nabla h) \right] + \alpha q_{wb} + \alpha q_{rb} = \alpha \frac{\partial (\phi \rho_b S_b)}{\partial t}. \quad (42b)$$

10 *Once S_g and p_b are known, S_b and p_g can be obtained from Equation (38) and from Equation*
 11 *(41), respectively.*

12 *All materials are assumed to be isotropic (Howarth and Christian-Frear 1997). Thus, the*
 13 *tensor K_l in Equation (25) has the form*

$$14 \quad \mathbf{K}_l = \begin{bmatrix} k_l & 0 \\ 0 & k_l \end{bmatrix}, \quad (43)$$

15 *where k_l is the permeability to fluid l for the particular material under consideration. For*
 16 *brine (i.e., fluid $l = b$), the permeability k_b is the same as the intrinsic permeability k in Table*
 17 *PA-2. For gas (i.e., fluid $l = g$), the permeability k_g is obtained by modifying the intrinsic*
 18 *permeability k to account for the Klinkenberg effect (Klinkenberg 1941). Specifically,*

$$19 \quad k_g = k \left(\frac{1 + bk^a}{p_g} \right), \quad (44)$$

20 *where $a = a_{klink}$ and $b = b_{klink}$ are gas- and formation-dependent constants. Values of*
 21 *$a_{klink} = -0.3410$ and $b_{klink} = 0.2710$ were determined from data obtained for MB 139*
 22 *(Christian-Frear 1996), with these values used for all regions in Figure PA-8. A pressure-*
 23 *dependent modification of k is used in the anhydrite MBs and in the DRZ in the presence of*
 24 *pressure-induced fracturing (see Section PA-4.2.4).*

1 *Gas density is computed using the Redlich-Kwong-Soave (RKS) equation of state, with the gas*
 2 *assumed to be pure hydrogen. For a pure gas, the RKS equation of state has the form (pp. 43-*
 3 *54, Walas 1985)*

$$4 \quad p_g = \frac{RT}{V-b} - \frac{a\alpha}{V(V+b)}, \quad (45)$$

5 *where*

$$6 \quad R = \text{gas constant} = 8.31451 \text{ J mol}^{-1} \text{ K}^{-1},$$

$$7 \quad T = \text{temperature (K)} = 300.15 \text{ K} (= 30^\circ \text{C}),$$

$$8 \quad V = \text{molar volume (m}^3 \text{ mol}^{-1}),$$

$$9 \quad a = 0.42747 R^2 T_c^2 / P_c,$$

$$10 \quad b = 0.08664 RT_c / P_c$$

$$11 \quad \alpha = \left[1 + (0.48508 + 1.55171\omega - 0.15613\omega^2)(1 - T_r^{0.5}) \right]^2$$

$$12 \quad \approx 1.202 \exp(-0.30288T_r) \quad \text{for hydrogen (Graboski and Daubert 1979),}$$

$$13 \quad T_c = \text{critical temperature (K)},$$

$$14 \quad P_c = \text{critical pressure (Pa)},$$

$$15 \quad T_r = T / T_c = \text{reduced temperature},$$

$$16 \quad \omega = \text{acentric factor}$$

$$17 \quad = 0 \text{ for hydrogen (Graboski and Daubert 1979).}$$

18 *For hydrogen, pseudo-critical temperature and pressure values of $T_c = 43.6 \text{ }^\circ\text{K}$ and*
 19 *$P_c = 2.047 \times 10^6 \text{ Pa}$ are used instead of the true values of these properties (Prausnitz 1969).*

20 *Equation (45) is solved for molar volume V . The gas density ρ_g then is given by*

$$21 \quad \rho_g = \frac{M_{w,H_2}}{V}, \quad (46)$$

22 *where M_{w,H_2} is the molecular weight of hydrogen (i.e., $2.01588 \times 10^{-3} \text{ kg/mol}$; see p. B-26,*
 23 *Weast 1969).*

24 *Brine density ρ_b is defined by Equation (25f), with $\rho_0 = 1230.0 \text{ kg/m}^3$ at a pressure of $p_{b0} =$*
 25 *$1.0132 \times 10^5 \text{ Pa}$ and $\beta_b = 2.5 \times 10^{-10} \text{ Pa}^{-1}$ (Roberts 1996). Porosity, ϕ , is used as defined by*

1 *Equation (25g) with two exceptions: in the repository (see Section PA-4.2.3) and in the MBs*
 2 *subsequent to fracturing (see Section PA-4.2.4). The values of ϕ_0 and β_f used in conjunction*
 3 *with Equation (25g) are listed in Table PA-2. The reference pressure p_{b0} in Equation (25g) is*
 4 *spatially-variable and corresponds to the initial pressures $p_b(x, y, -5)$ (see Section PA-4.2.2).*
 5 *The gas and brine viscosities μ_l , $l = g, b$ in Equation (25a) and Equation (25b) were assumed*
 6 *to have values of $\mu_g = 8.92 \times 10^{-6}$ Pa s (Vargaftik 1975) and $\mu_b = 2.1 \times 10^{-3}$ Pa s (McTigue*
 7 *1993).*

8 *The terms q_{wg} , q_{rg} , q_{wb} , and q_{rb} in Equation (25a) and Equation (25b) relate to well injection*
 9 *or removal (i.e., q_{wg} , q_{wb}) and reaction production or consumption (i.e., q_{rg} , q_{rb}) of gas and*
 10 *brine, with positive signs corresponding to injection or production and negative signs*
 11 *corresponding to removal or consumption. No injection or removal of gas or brine is assumed*
 12 *to take place within the region in Figure PA-8. Thus, q_{wg} and q_{wb} are equal to zero. Further,*
 13 *no gas consumption occurs (see below), and gas production has the potential to occur (due to*
 14 *corrosion of steel or microbial degradation of cellulosic, plastic, or rubber (CPR) materials)*
 15 *only in the waste disposal regions of the repository (i.e., Waste Panel, South RoR, and North*
 16 *RoR in Figure PA-8). Thus,*

$$17 \quad q_{rg} \geq 0 \quad \text{in waste disposal regions of Figure PA-8} \\ 18 \quad \quad \quad = 0 \quad \text{elsewhere.} \quad (47)$$

19 *In actuality, some gas consumption does occur due to the reaction of CO_2 with the MgO in the*
 20 *waste panels. This gas consumption is not modeled explicitly and is accounted for by reducing*
 21 *the gas generation rate q_{rg} , as discussed in Section PA-4.2.5. Finally, no brine production*
 22 *occurs, and brine consumption has the potential to occur (due to the consumption of brine*
 23 *during the corrosion of steel) only in the waste disposal regions of the repository. Thus,*

$$24 \quad q_{rb} \leq 0 \quad \text{in waste disposal regions of Figure PA-8} \\ 25 \quad \quad \quad = 0 \quad \text{elsewhere.} \quad (48)$$

26 *More detail on the definition of q_{rg} and q_{rb} is provided in Section PA-4.2.5.*

27 *PA-4.2.2 Initial Conditions*

28 *In each two-phase flow simulation, a short period of time representing disposal operations is*
 29 *simulated. This period of time is called the start-up period and covers five years from $t = -5$*
 30 *years to 0 years, corresponding to the amount of time a typical panel is expected to be open*
 31 *during disposal operations. All grid locations require initial brine pressure and gas saturation*
 32 *at the beginning of the simulation ($t = -5$ years).*

33 *The Rustler Formation and overlying units (except in the shaft) are modeled as horizontal*
 34 *with spatially constant initial pressure in each layer (see Figure PA-8). Table PA-4 lists the*
 35 *initial brine pressure p_b and gas saturation S_g for the Rustler Formation.*

1

Table PA-4. Initial Conditions in the Rustler Formation

Name	Mesh Row (Figure PA-8)	$p_b(x, y, -5), Pa$	$S_g(x, y, -5)$
Santa Rosa Formation	33	1.013250×10^5	$1 - Sbr = 0.916$
Santa Rosa Formation	32	1.013250×10^5	$1 - Sbr = 0.916$
Dewey Lake	31	1.013250×10^5	$1 - Sbr = 0.916$
Dewey Lake	30	7.355092×10^5	$1 - Sbr = 0.916$
49er	29	1.473284×10^6	0
Magenta	28	9.170000×10^5	0
Tamarisk	27	1.827087×10^6	0
Culebra	26	8.220000×10^5	0
Los Medaños Unnamed	25	2.274809×10^6	0

2 *The Salado Formation (mesh rows 3 – 24 in Figure PA-8) is assumed to dip uniformly $\theta = 1^\circ$*
 3 *downward from north to south (right to left in Figure PA-8). Except in the repository*
 4 *excavations and in the shaft, brine is assumed initially (i.e., at -5 years) to be in hydrostatic*
 5 *equilibrium relative to an uncertain initial pressure $p_{b,ref}$ (SALPRES, see Table PA-17) at a*
 6 *reference point located at center of shaft at the elevation of the midpoint of MB139, which is*
 7 *the center of cell 1266 in Figure PA-10). This gives rise to the condition*

$$8 \quad p_b(x, y, -5) = p_{b0} + \left(\frac{1}{\beta_b} \right) \ln \left[\frac{\rho_b(x, y, -5)}{\rho_{b0}} \right], \quad (49)$$

9 *where*

$$10 \quad \rho_b(x, y, -5) = \frac{1}{g \beta_b \left[y_e - \Phi(x_{ref}, y_{ref}, -5) + \frac{1}{g \beta_b \rho_{b0}} \right]}$$

$$11 \quad \Phi(x_{ref}, y_{ref}, -5) = y_{ref} + \frac{1}{g \beta_b} \left[\frac{1}{\rho_{b0}} - \frac{1}{\rho_b(x_{ref}, y_{ref}, -5)} \right]$$

$$12 \quad \rho_b(x_{ref}, y_{ref}, -5) = \rho_{b0} \exp \left[-\beta_b (p_{b,ref} - p_{b0}) \right]$$

$$13 \quad y_e = y_{ref} + h(x, y) = y_{ref} + (x - x_{ref}) \sin \theta + (y - y_{ref}) \cos \theta \quad (\text{see Equation (27)})$$

1 *and $\rho_{b0} = 1220 \text{ kg/m}^3$, $\beta_b = 3.1 \times 10^{-10} \text{ Pa}^{-1}$, $g = 9.80665 \text{ m/s}^2$, and $p_{b0} = 1.01325 \times 10^5 \text{ Pa}$.*
 2 *In the Salado Formation, initial gas saturation $S_g(x, y, -5) = 0$.*

3 *The Castile Formation (mesh rows 1 and 2) is modeled as horizontal, and initial brine*
 4 *pressure is spatially constant within each layer, except that the brine reservoir is treated as a*
 5 *different material from rest of Castile and has a different initial pressure. Specifically, outside*
 6 *the brine reservoir,*

$$7 \quad p_b(x, y, -5) = \begin{cases} 1.54445 \times 10^7 \text{ Pa} & \text{in mesh row 2} \\ 1.65151 \times 10^7 \text{ Pa} & \text{in mesh row 1} \end{cases} \quad (50)$$

8 *Within the reservoir, $p_b(x, y, -5) = BPINTPRS$, the uncertain initial pressure in the*
 9 *reservoir (see Table PA-17). Initial gas saturation $S_g(x, y, -5) = 0$.*

10 *Within the shaft (areas Upper Shaft, Lower Shaft, and CONC_MON) and panel closures*
 11 *(areas CONC_PCS and DRF_PCS), $p_b(x, y, -5) = 1.01325 \times 10^5 \text{ Pa}$ and*
 12 *$S_g(x, y, -5) = 1 \times 10^{-7}$. Within the excavated areas (Waste Panel, South RoR, and North*
 13 *RoR, Ops and Exp), $p_b(x, y, -5) = 1.01325 \times 10^5 \text{ Pa}$ and $S_g(x, y, -5) = 0$.*

14 *At the end of the initial five-year start-up period and the beginning of the regulatory period (t*
 15 *$= 0$ years), brine pressure and gas saturation are reset in the shaft, panel closures, and*
 16 *excavated areas. In the shaft (areas Upper Shaft, Lower Shaft, and CONC_MON) and panel*
 17 *closures (areas CONC_PCS and DRF_PCS), $p_b(x, y, 0) = 1.01325 \times 10^5 \text{ Pa}$ and*
 18 *$S_g(x, y, 0) = 1 \times 10^{-7}$. In the waste disposal regions (areas Waste Panel, South RoR, and*
 19 *North RoR), $p_b(x, y, 0) = 1.01325 \times 10^5 \text{ Pa}$ and $S_g(x, y, 0) = 0.985$. In the other excavated*
 20 *areas, $p_b(x, y, 0) = 1.01325 \times 10^5 \text{ Pa}$ and $S_g(x, y, 0) = 1.0$.*

21 *PA-4.2.3 Creep Closure of Repository*

22 *The porosity of the waste disposal regions and neighboring access drifts (i.e., Waste Panel,*
 23 *South RoR, North RoR, and DRF_PCS in Figure PA-8) is assumed to change through time*
 24 *due to creep closure of the halite surrounding the excavations. The equations on which*
 25 *BRAGFLO is based do not incorporate this type of deformation. Therefore, the changes in*
 26 *repository porosity due to halite deformation are modeled in a separate analysis with the*
 27 *geomechanical program SANTOS, which implements a quasi-static, large-deformation, finite-*
 28 *element procedure (Stone 1997). Interpolation procedures are then used with the SANTOS*
 29 *results to define ϕ within the repository as a function of time, pressure, and gas generation*
 30 *rate.*

31 *For more information on the generation of the porosity surface for BRAGFLO for the CRA-*
 32 *2004 PA, see Appendix PA, Attachment PORSURF.*

1 **PA-4.2.4 Fracturing of Marker Beds and Disturbed Rock Zone**

2 **Fracturing within the anhydrite MBs (i.e., regions MB 138, Anhydrite AB, and MB 139 in**
 3 **Figure PA-8) and in the DRZ (region DRZ in Figure PA-8) is assumed to occur at pressures**
 4 **slightly below lithostatic pressure and is implemented through a pressure-dependent**
 5 **compressibility $\beta_f(p_b)$ (Mendenhall and Gerstle 1995). Specifically, fracturing of the MBs**
 6 **begins at a brine pressure of**

7
$$p_{bi} = p_{b0} + \Delta p_i, \quad (51)$$

8 **where p_{bi} and p_{b0} are spatially dependent (i.e., $p_{b0} = p_b(x, y, 0)$ as in Section PA-4.2.2) and**
 9 **$\Delta p_i = 2 \times 10^5$ Pa.**

10 **Fracturing ceases at a pressure of**

11
$$p_{ba} = p_{b0} + \Delta p_a \quad (52)$$

12 **and a fully-fractured porosity of**

13
$$\phi(p_{ba}) = \phi_a = \phi_0 + \Delta \phi_a, \quad (53)$$

14 **where $\Delta p_a = 3.8 \times 10^6$ Pa, ϕ_0 is spatially dependent (Table PA-2), and $\Delta \phi_a = 0.04, 0.24,$ and**
 15 **0.04 for anhydrite materials S_MB138, S_ANH_AB and $S_MB139,$ respectively.**

16 **Compressibility β_f is a linear function**

17
$$\beta_f(p_b) = \beta_f + \left(\frac{p_b - p_{bi}}{p_{ba} - p_{bi}} \right) (\beta_{fa} - \beta_f) \quad (54)$$

18 **of brine pressure for $p_{bi} \leq p_b \leq p_{ba}$, with β_{fa} defined so that the solution ϕ of**

19
$$\frac{d\phi}{dp_b} = \beta_{fa}(p_b)\phi, \quad \text{where } \phi(p_{bi}) = \phi_0 \exp[\beta_f(p_{bi} - p_{b0})] \quad (55)$$

20 **satisfies $\phi(p_{ba}) = \phi_a$; specifically, β_{fa} is given by**

21
$$\beta_{fa} = \beta_f \left[1 - \frac{2(p_{ba} - p_{b0})}{p_{ba} - p_{bi}} \right] + \left[\frac{2}{p_{ba} - p_{bi}} \right] \ln \left(\frac{\phi_a}{\phi_0} \right). \quad (56)$$

22 **The permeability $k_f(p_b)$ of fractured material at brine pressure p_b is related to the**
 23 **permeability of unfractured material at brine pressure p_{bi} by**

$$k_f(p_b) = \left[\frac{\phi(p_b)}{\phi(p_{bi})} \right]^n k, \quad (57)$$

where k is the permeability of unfractured material (i.e., at p_{bi}) and n is defined so that $k_f(p_b) = 1 \times 10^{-9} \text{ m}^2$ (i.e., n is a function of k , which is an uncertain input to the analysis; see ANHPRM in Table PA-17). When fracturing occurs, $k_f(p_b)$ is used instead of k in the definition of the permeability tensor K_l in Equation (43) for the fractured areas of the anhydrite MBs.

Fracturing is also modeled in the DRZ. The implementation of the fracture model is the same as for the anhydrite materials. In this case, fracturing would be in halite rather than anhydrite, but because of the limited extent of the DRZ and the proximity of the nearby interbeds, this representation was deemed acceptable by the Salado Flow Peer Review panel (Caporuscio et al. 2003).

PA-4.2.5 Gas Generation

Gas production is assumed to result from anoxic corrosion of steel and microbial degradation of CPR materials. Thus, the gas generation rate q_{rg} in Equation (25a) is of the form

$$q_{rg} = q_{rgc} + q_{rgm}, \quad (58)$$

where q_{rgc} is the rate of gas production per unit volume of waste ($\text{kg}/\text{m}^3/\text{s}$) due to anoxic corrosion of Fe-base metals and q_{rgm} is the rate of gas production per unit volume of waste ($\text{kg}/\text{m}^3/\text{s}$) due to microbial degradation of CPR materials. Furthermore, q_{rb} in Equation (25b) is used to describe the consumption of brine during the corrosion process.

Gas generation takes place only within the waste disposal regions (i.e., Waste Panel, South RoR, and North RoR in Figure PA-8) and all the generated gas is assumed to have the same properties as H_2 (see discussion in Attachment MASS, Section MASS-3.2). In the CCA PA and the CRA-2004 PA, the consumable materials are assumed to be homogeneously distributed throughout the waste disposal regions (i.e., the concentration of Fe-base metals and of CPR materials in the waste is a constant; see Appendix TRU WASTE, Table TRU WASTE-1). A separate analysis examined the potential effects on PA results of spatially-varying concentrations of Fe-base metals and CPR materials, and concluded that PA results are not affected by representing these materials with spatially-varying concentrations (see Attachment MASS, Section MASS.21).

The rates q_{rgc} , q_{rb} and q_{rgm} are defined by

$$q_{rgc} = \left(R_{ci} S_{b,eff} + R_{ch} S_g^* \right) D_s \rho_{Fe} X_c (H_2 | Fe) M_{H_2} \quad (59)$$

$$q_{rb} = \left(q_{rgc} / M_{H_2} \right) X_c \left(H_2O | H_2 \right) M_{H_2O} \quad (60)$$

$$q_{rgm} = \left(R_{mi} S_{b,eff} + R_{mh} S_g^* \right) D_c y \left(H_2 | C \right) M_{H_2}, \quad (61)$$

3 *where*

4 D_s = *surface area concentration of steel in the repository ((m² surface area steel)/*
 5 *(m³ disposal volume)),*

6 D_c = *mass concentration of cellulose in the repository ((kg biodegradable*
 7 *material)/(m³ of disposal volume)),*

8 M_{H_2} = *molecular weight of H₂ (kg H₂/mol H₂),*

9 M_{H_2O} = *molecular weight of H₂O (kg H₂O/mol H₂O),*

10 R_{ci} = *corrosion rate under inundated conditions (m/s),*

11 R_{ch} = *corrosion rate under humid conditions (m/s),*

12 R_{mi} = *rate of cellulose biodegradation under inundated conditions*
 13 *(mol C₆H₁₀O₅/kg C₆H₁₀O₅/s),*

14 R_{mh} = *rate of cellulose biodegradation under humid conditions*
 15 *(mol C₆H₁₀O₅/kg C₆H₁₀O₅/s),*

16 $S_{b,eff}$ = *effective brine saturation due to capillary action in the waste materials (see*
 17 *Equation (78) in Section PA-4.2.6),*

$$S_g^* = \begin{cases} 1 - S_{b,eff} & \text{if } S_{b,eff} > 0 \\ 0 & \text{if } S_{b,eff} = 0 \end{cases}$$

19 $X_c \left(H_2 | Fe \right)$ = *stoichiometric coefficient for gas generation due to corrosion of steel, i.e.,*
 20 *moles of H₂ produced by the corrosion of 1 mole of Fe (mol H₂ / mol Fe),*

21 $X_c \left(H_2O | H_2 \right)$ = *stoichiometric coefficient for brine consumption due to corrosion of steel,*
 22 *i.e., moles of H₂O consumed per mole of H₂ generated by corrosion*
 23 *(mol H₂O / mol H₂),*

1 $y(H_2|C)$ = average stoichiometric factor for microbial degradation of cellulose, i.e., the
 2 moles of H_2 generated per mole of carbon consumed by microbial action
 3 (mol H_2 /mol $C_6H_{10}O_5$), and

4 ρ_{Fe} = molar density of steel (mol/m³).

5 The products $R_{ci} D_s \rho_{Fe} X_c$, $R_{ch} D_s \rho_{Fe} X_c$, $R_{mi} D_c y$, and $R_{mh} D_c y$ in Equation (59) and
 6 Equation (61) define constant rates of gas generation (mol/m³/s) that continue until the
 7 associated substrate (i.e. steel or cellulose) is exhausted (i.e., zero order kinetics). The terms
 8 $S_{b,eff}$ and S_g^* in Equation (59) and Equation (61), which are functions of location and time,
 9 correct for the amount of substrate that is exposed to inundated and humid conditions,
 10 respectively. All the corrosion and microbial action is assumed to cease when no brine is
 11 present, which is the reason that 0 replaces $S_g = 1$ in the definition of S_g^* . In the CRA-2004
 12 PA, $R_{ch} = 0$ and R_{ci} , R_{mh} , and R_{mi} are defined by uncertain variables (see WGRCOR,
 13 WGRMICH, WGRMICI in Table PA-17). Further, $M_{H_2} = 2.02 \times 10^{-3}$ kg/mol (pp. 1-7, 1-8,
 14 Lide 1991), $M_{H_2O} = 1.80 \times 10^{-2}$ kg/mol (pp. 1-7, 1-8, Lide 1991), $\rho_{Fe} = 1.41 \times 10^5$ mol/m³
 15 (Telander and Westerman 1993), and D_s , D_c , $X_c(H_2O|H_2)$, $X_c(H_2|Fe)$ and $y(H_2|C)$
 16 are discussed below.

17 The concentration D_s in Equation (59) is defined by

$$18 \quad D_s = A_d n_d / V_R, \quad (62)$$

19 where

20 A_d = surface area of steel associated with a waste disposal drum (m²/drum),

21 V_R = initial volume of the repository (m³), and

22 n_d = number of waste drums required to hold all the waste emplaced in the
 23 repository (drums).

24 In the CRA-2004 PA, $A_d = 6$ m²/drum (Vol. 3, WIPP PA 1991-1992), $V_R = 438,406$ m³ (Stein
 25 2002b), and $n_d = 818,498$ drums ($n_d = V_R \times DROOM / VROOM$, where DROOM is the
 26 number of drums per room {6804 drums} and VROOM is the volume of each room
 27 {3644 m³}).

28 The biodegradable materials to be disposed of at the WIPP consist of cellulosic materials,
 29 rubbers, and both waste plastics and container plastics. Cellulosics have been demonstrated
 30 experimentally to be the most biodegradable among these materials (Francis et al. 1997). The
 31 occurrence of significant microbial gas generation in the repository will depend on: (1)

1 *whether microbes capable of consuming the emplaced organic materials will be present and*
 2 *active; (2) whether sufficient electron acceptors will be present and available; and (3) whether*
 3 *enough nutrients will be present and available. Given the uncertainties in these factors, a*
 4 *probability of 0.5 is assigned to the occurrence of microbial gas generation (see WMICDFLG*
 5 *in Table PA-17). Furthermore, two factors may increase the biodegradability of plastics and*
 6 *rubbers: long time scale and cometabolism. Over a time scale of 10,000 years, the chemical*
 7 *properties of plastics and rubbers may change, increasing their biodegradability.*
 8 *Cometabolism means that microbes may degrade organic compounds, but do not use them as*
 9 *a source of energy, which is derived from other substrates. Both of these factors are highly*
 10 *uncertain and therefore a probability of 0.5 is assigned to biodegradation of plastics and*
 11 *rubbers conditional on the occurrence of biodegradation of cellulosic materials (see*
 12 *WMICDFLG in Table PA-17). In cases where biodegradation of rubbers and plastics occur,*
 13 *rubbers and plastics are converted to an equivalent quantity of cellulose based on their*
 14 *carbon equivalence (Wang and Brush 1996a). This produces the density calculation*

$$D_c = \begin{cases} m_{cel} / V_R & \text{for biodegradation of cellulose only} \\ (m_{cel} + m_r + 1.7 m_p) / V_R & \text{for biodegradation of CPR materials,} \end{cases} \quad (63)$$

15 *where m_{cel} is mass of cellulose (kg), m_r is the mass of rubbers (kg), and m_p is the mass of*
 16 *plastics (kg). The factor of 1.7 converts all plastics to an equivalent quantity of cellulose*
 17 *based on carbon equivalence. In the CRA-2004 PA,*

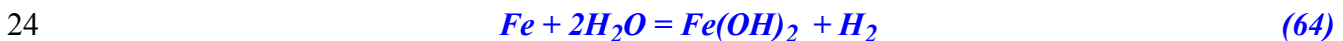
$$18 \quad m_{cel} = [(58.0 \text{ kg/m}^3 \times 168,485 \text{ m}^3) + (4.5 \text{ kg/m}^3 \times 7,079 \text{ m}^3)] = 9.8 \times 10^6 \text{ kg,}$$

$$19 \quad m_r = [(14.0 \text{ kg/m}^3 \times 168,485 \text{ m}^3) + (3.1 \text{ kg/m}^3 \times 7,079 \text{ m}^3)] = 2.4 \times 10^6 \text{ kg}$$

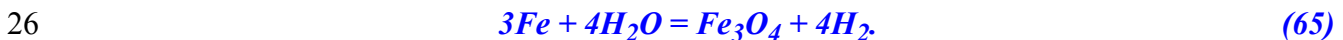
$$20 \quad m_p = [(58.0 \text{ kg/m}^3 \times 168,485 \text{ m}^3) + (6.3 \text{ kg/m}^3 \times 7,079 \text{ m}^3)] = 9.8 \times 10^6 \text{ kg.}$$

21 *Values for the density for CPR materials can be found in Appendix DATA, Attachment F.*

22 *The most plausible corrosion reactions after closure of the WIPP are believed to be (Wang*
 23 *and Brush 1996a)*



25 *and*



27 *When linearly weighted by the factors x and $1 - x$ ($0 \leq x \leq 1$), the two preceding reactions*
 28 *become*



where x and $1-x$ are the fractions of iron consumed in the reactions in Reaction (64) and Reaction (65), respectively. Although magnetite (Fe_3O_4) has been observed to form on iron as a corrosion product in low-Mg anoxic brines at elevated temperatures (Telander and Westerman 1997) and in oxic brine (Haberman and Frydrych 1988), there is no evidence that it will form at WIPP repository temperatures. If Fe_3O_4 were to form, H_2 would be produced (on a molar basis) in excess of the amount of Fe consumed. However, anoxic corrosion experiments (Telander and Westerman 1993) did not indicate the production of H_2 in excess of the amount of Fe consumed. Therefore, the stoichiometric factor x in Reaction (66) is set to 1.0 (i.e., $x = 1$), which implies that Reaction (64) represents corrosion. Thus, the stoichiometric factor for corrosion is

$$X_c(H_2|Fe) = (4-x)/3 = 1 \text{ mol/mol}, \quad (67)$$

which implies that one mole of H_2 is produced for each mole of iron consumed, and the stoichiometric factor for brine consumption is

$$X_c(H_2O|H_2) = (4+2x)/3 = 2 \text{ mol/mol}, \quad (68)$$

which implies that two moles of H_2O are consumed for each mole of H_2 produced. The most plausible biodegradation reactions after closure of the WIPP are believed to be (Wang and Brush 1996a)



Accumulation of CO_2 produced by the above reactions could decrease pH and thus increase actinide solubility in the repository (Wang and Brush 1996b). To improve WIPP performance, a sufficient amount of MgO will be added to the repository to remove CO_2 (Bynum et al. 1997). The consumption of CO_2 by MgO in the repository takes place by the reactions outlined in Section 6.4.3.4. The removal of CO_2 by MgO is not explicitly represented in the BRAGFLO code. Rather, the effect of CO_2 consumption is accounted for by modifying the stoichiometry of Reaction (69) to remove the CO_2 from the mass of gas produced by microbial action.

The average stoichiometry of Reaction (69), is



1 where the average stoichiometric factor y in Reaction (70) represents the number of moles of
 2 gas produced and retained in the repository from each mole of carbon consumed. This factor
 3 y depends on the extent of the individual biodegradation pathways in Reaction (69), and the
 4 consumption of CO_2 by MgO . An range of values for y is estimated by considering the
 5 maximum mass of gas that can be produced from consumption of cellulosics (M_{cel}) and Fe-
 6 base metals (M_{Fe}), and is derived as follows (Wang and Brush 1996b).

7 Estimates of the maximum quantities M_{cel} and M_{Fe} (mol) of cellulosics (i.e., $\text{C}_6\text{H}_{10}\text{O}_5$) and
 8 steels that can be potentially consumed in 10,000 years are given by

$$9 \quad M_{cel} = \min \left\{ \frac{6000 m_{cel}}{162}, 3.2 \times 10^{11} R_m m_{cel} \right\} \quad (71)$$

$$10 \quad M_{Fe} = \min \left\{ \frac{1000 m_{Fe}}{56}, 4.4 \times 10^{16} R_{ci} A_d n_d \right\}, \quad (72)$$

11 where m_{cel} and m_{Fe} are the masses (kg) of cellulosics (see Equation (63) for definition) and
 12 steels initially present in the repository. The mass of cellulosics that can be consumed is
 13 determined by the uncertain parameter $WMICDFLG$ (see Table PA-17). The mass of steels,
 14 $m_{Fe} = 5.15 \times 10^7$ kg; this value is calculated as:

$$15 \quad V_{CH} (\rho_{WCH} + \rho_{CCH}) + V_{RH} (\rho_{WRH} + \rho_{CRH}), \quad (73)$$

16 where V_{CH} and V_{RH} are the volumes of CH- and RH-TRU waste, ρ_{WCH} and ρ_{WRH} are the
 17 iron densities in CH- and RH-TRU waste, and ρ_{CCH} and ρ_{CRH} are the iron densities of the
 18 containers of CH- and RH-TRU waste (Appendix DATA, Attachment F). The terms
 19 $6000 m_{cel}/162$ and $1000 m_{Fe}/56$ in Equation (71) and Equation (72) equal the inventories in
 20 moles of cellulosics and steel, respectively. The terms $3.2 \times 10^{11} R_m m_{cel}$ and
 21 $4.4 \times 10^{16} R_{ci} A_d n_d$ equal the maximum amounts of cellulosics and steel that could be
 22 consumed over 10,000 years. In Equation (71), $R_m = \max \{ R_{mh}, R_{mi} \}$, where R_{mh} and R_{mi}
 23 are defined by uncertain variables (see $WGRMICH$ and $WGRMICI$ in Table PA-17,
 24 respectively), and $3.2 \times 10^{11} = (3.15569 \times 10^7 \text{ s/yr}) (10^4 \text{ yr})$. In Equation (72), $A_d n_d$ is the total
 25 surface area of all drums (m^2) and the factor $4.4 \times 10^{16} = (3.15569 \times 10^7 \text{ s/yr}) (10^4 \text{ yr})$
 26 $(1.41 \times 10^5 \text{ mol/m}^3)$, where $\rho_{Fe} = 1.41 \times 10^5 \text{ mol/m}^3$ (see Equation (59)) (Telander and
 27 Westerman 1993), converts the corrosion rate from m/s to $\text{mol/m}^2/\text{s}$.

28 A range of possible values for the average stoichiometric factor y in Reaction (70) can be
 29 obtained by considering individual biodegradation pathways involving M_{cel} and accounting
 30 for the removal of CO_2 by the MgO . Two extreme cases corresponding to the maximum and
 31 minimum values of y exist: (1) there is no reaction of microbially produced H_2S with ferrous
 32 metals and metal corrosion products, and (2) there is a complete reaction of microbially

1 *produced H₂S with ferrous metals and metal corrosion products. If no H₂S is consumed by*
 2 *reactions with Fe and Fe-corrosion products, the maximum quantity of microbial gas will be*
 3 *retained in the repository and therefore the maximum value for y results. Thus, the maximum*
 4 *value of y can be estimated by averaging the gas yields for all reaction pathways to produce*

$$5 \quad y_{max} = \frac{\frac{2.4 M_{NO_3}}{4.8} + \frac{3 M_{SO_4}}{3} + 0.5 \left(M_{cel} - \frac{6 M_{NO_3}}{4.8} - \frac{6 M_{SO_4}}{3} \right)}{M_{cel}}, \quad (74)$$

6 *where M_{NO_3} and M_{SO_4} are the quantities of NO_3^- and SO_4^{2-} (in moles) initially present in*
 7 *the repository. Specifically, $M_{NO_3} = 2.51 \times 10^7$ mol and $M_{SO_4} = 4.21 \times 10^5$ mol (Appendix*
 8 *DATA, Attachment F, Table DATA-F-35).*

9 *If H₂S reacts with Fe and Fe- corrosion products, a significant quantity or perhaps all of the*
 10 *microbially produced H₂S would be consumed to produce FeS, which would result in the*
 11 *minimum value of y. Specifically,*

$$12 \quad y_{min} = \frac{\frac{2.4 M_{NO_3}}{4.8} + \frac{3 M_{SO_4}}{3} + 0.5 \left(M_{cel} - \frac{6 M_{NO_3}}{4.8} - \frac{6 M_{SO_4}}{3} \right) - G}{M_{cel}} = y_{max} - \frac{G}{M_{cel}}, \quad (75)$$

13 *where*

$$14 \quad G = \min \left\{ \frac{3 M_{SO_4}}{3}, M_{Fe} \right\}. \quad (76)$$

15 *The stoichiometric factor y value is believed to be located within the interval $[y_{min}, y_{max}]$.*

16 *That is,*

$$17 \quad y = y_{min} + \beta(y_{max} - y_{min}), \quad 0 \leq \beta \leq 1. \quad (77)$$

18 *The variable β in the preceding equation is treated as an uncertain quantity in the CRA-2004*
 19 *PA (see WFBETCEL in Table PA-17).*

20 **PA-4.2.6 Capillary Action in the Waste**

21 *Capillary action (wicking) refers to the ability of a material to carry a fluid by capillary forces*
 22 *above the level it would normally seek in response to gravity. In the current analysis, this*
 23 *phenomena is accounted for by defining an effective saturation given by*

$$S_{b,eff} = \begin{cases} S_b + S_{wick} & \text{if } 0 < S_b < 1 - S_{wick} \\ 0 & \text{if } S_b = 0 \\ 1 & \text{if } S_b > 1 - S_{wick} \end{cases}, \quad (78)$$

where

$S_{b,eff}$ = effective brine saturation,

S_b = brine saturation,

S_{wick} = wicking saturation.

The effective saturation is used on a grid block basis within all waste regions (Waste Panel, South RoR, and North RoR in Figure PA-8). The wicking saturation, S_{wick} , is treated as an uncertain variable (see WASTWICK in Table PA-17). The effective brine saturation $S_{b,eff}$ is only used in the calculation of the corrosion of steel (Equation (59)) and the microbial degradation of cellulose (Equation (61)) and does not directly affect the two-phase flow calculations indicated.

PA-4.2.7 Shaft Treatment

The WIPP excavation includes four shafts that connect the repository region to the surface: the air intake shaft, salt handling shaft, waste handling shaft, and exhaust shaft. In both the CCA PA and the CRA-2004 PA, these four shafts are modeled as a single shaft. The rationale for this modeling treatment is set forth in WIPP PA 1992-1993 (Section 2.3, Vol. 5).

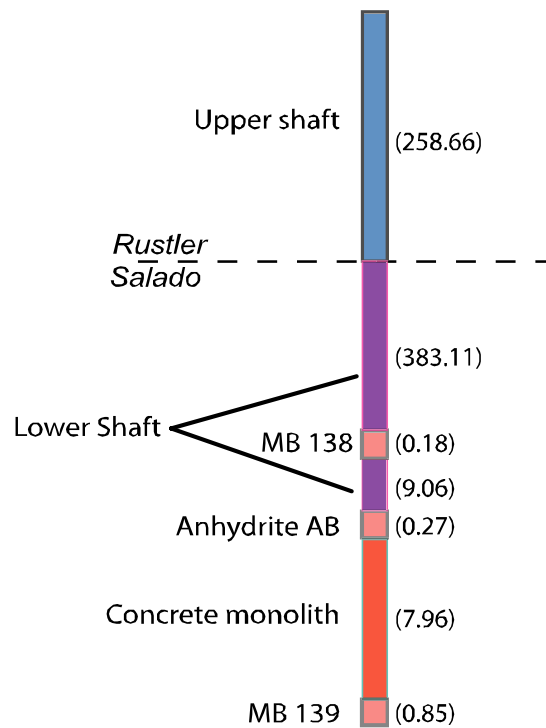
A shaft seal model is included in the CRA-2004 grid (column 43 in Figure PA-8), but it is implemented in a simpler fashion than for the CCA PA. A detailed description of the new implementation and its parameters are discussed in AP-094 (James and Stein 2002) and the resulting analysis report (James and Stein 2003). The final version of the shaft seal model used in the CRA-2004 PA is described by Stein and Zelinski (2003a); this model was approved by the Salado Flow Peer Review panel (Caporuscio et al. 2003).

The planned design of the shaft seals involves numerous materials including earth, crushed salt, clay, asphalt, and Salado Mass Concrete (SMC) (CCA Appendix SEAL). The design is intended to control both short-term and long-term fluid flow through the Salado portion of the shafts. For the CCA PA, each material in the shaft seal was represented in the BRAGFLO grid. Analysis of the flow results from the CCA PA and subsequent 1997 Performance Assessment Verification Test (PAVT) (SNL 1997) indicated that no significant flows of brine or gas occurred in the shaft during the 10,000-year regulatory period. As a result of these analyses, a simplified shaft seal model was developed for the CRA-2004 PA.

A conceptual representation of the simplified shaft seal system used in CRA-2004 PA is shown in Figure PA-11. The simplified model divides the shaft into three sections: an upper section (shaft seal above the Salado), a lower section (within the Salado), and a concrete monolith section within the repository horizon. A detailed discussion on how the material properties

1 *were assigned for the simplified shaft seal model is included in James and Stein (2003). The*
 2 *permeability value used to represent the upper and lower sections is defined as the harmonic*
 3 *mean of the permeability of the component materials in the detailed shaft seal model*
 4 *(including permeability adjustments made for the DRZ assumed to surround the lower shaft*
 5 *seal section within the Salado). Porosity is defined as the thickness-weighted mean porosity of*
 6 *the component materials. Other material properties are described in James and Stein (2003).*

7 *The lower section of the shaft experiences a change in material properties at 200 years. This*
 8 *change simulates the consolidation of the seal materials within the Salado and results in a*
 9 *significant decrease in permeability. This time was chosen as a conservative overestimate of*
 10 *the amount of time expected for this section of the shaft to become consolidated. The concrete*
 11 *monolith section of the shaft is unchanged from the CCA PA and is represented as being*
 12 *highly permeable for 10,000 years to ensure that fluids can access the north end (operations*
 13 *and experimental areas) in the model. In three thin regions at the stratigraphic position of the*
 14 *anhydrite MBs, the shaft seal is modeled as MB material (Figure PA-11). This model feature*
 15 *is included so that fluids flowing in the DRZ and MB fractures can access the interbeds to the*
 16 *north of the repository “around” the shaft seals. Because these layers are so thin, they have*
 17 *virtually no effect on the effective permeability of the shaft seal itself.*

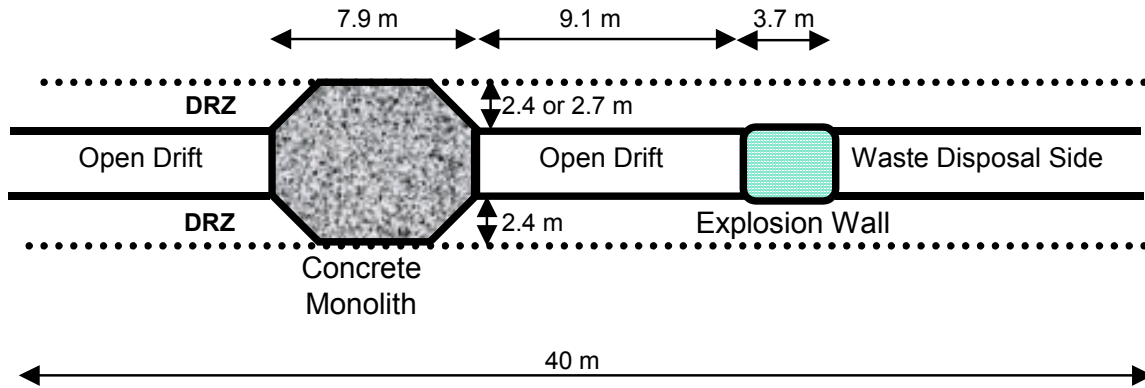


18
 19 *Figure PA-11. Schematic View of the Simplified Shaft Model.*

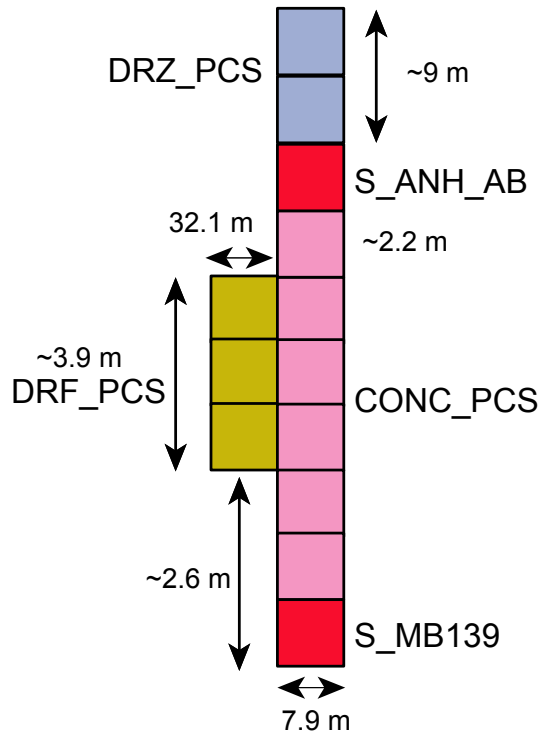
20 *The simplified shaft model was tested in the AP-106 analysis (Stein and Zelinski 2003a),*
 21 *which supported the Salado Flow Peer Review. The results of the AP-106 analysis*
 22 *demonstrated that vertical brine flow through the simplified shaft model was comparable to*
 23 *brine flows seen through the detailed shaft model used in the CCA PA and subsequent PAVT*
 24 *calculations.*

1 **PA-4.2.8 Option D Panel Closures**

2 *The CRA-2004 PA includes panel closures models that represent the Option D panel closure*
 3 *design (Section 6.4.3). Option D closures (Figure PA-12) are designed to allow minimal fluid*
 4 *flow between panels. The CRA-2004 PA explicitly represents selected Option D panel closures*
 5 *in the computational grid using a model that was approved by the Salado Flow Peer Review*
 6 *Panel (Caporuscio et al. 2003). The Option D panel closure design has several components:*
 7 *an SMC monolith, which extends into the DRZ in all directions, an empty drift section, and a*
 8 *block and mortar explosion wall (Figure PA-13). Each set of panel closures are represented in*
 9 *the BRAGFLO grid by four materials in 13 grid cells:*



10 **Figure PA-12. Schematic Side View of Option D Panel Closure.**



12 **Figure PA-13. Representation of Option D Panel Closures in the BRAGFLO Grid.**

- 1 • *Six cells of panel closure concrete (area CONC_PCS, material CONC_PCS),*
- 2 • *One cell above and one cell below the concrete material consisting of MB anhydrite*
- 3 *(areas MB 139 and Anhydrite AB, materials S_MB139 and S_ANH_AB, respectively),*
- 4 • *Two cells of healed DRZ above Anhydrite AB above the panel closure system (PCS)*
- 5 *(area DRZ_PCS, material DRZ_PCS), and*
- 6 • *Three cells of empty drift and explosion wall (area DRF_PCS, material DRF_PCS).*

7 *Properties for the materials comprising the panel closure system are listed in Table PA-2.*

8 *PA-4.2.8.1 Panel Closure Concrete*

9 *The Option D panel closure design requires the use of a salt-saturated concrete, identified as*
10 *SMC, as specified for the shaft seal system. The design of the shaft seal system and the*
11 *properties of SMC are described in Hurtado et al. (1997). The BRAGFLO grid incorporates*
12 *the material, CONC_PCS, which is assigned the material properties of undegraded SMC and*
13 *is used to represent the concrete portion of the Option D panel closure system (Figure PA-8).*
14 *A double-thick concrete segment is used to represent the northernmost set of panel closures*
15 *(between the north rest of repository and the operations area). This feature is meant to*
16 *represent the two sets of panel closures in series that will be emplaced between the waste filled*
17 *repository and the shaft.*

18 *PA-4.2.8.2 Panel Closure Abutment with Marker Beds*

19 *In the BRAGFLO grid, regions where the Option D panel closures intersect the MBs are*
20 *represented as blocks of MB material (Figure PA-8). This representation is warranted for two*
21 *reasons:*

- 22 *1. The MB material has a very similar permeability distribution (10^{-21} to $10^{-17.1}$ m²) as*
23 *the concrete portion of the Option D panel closures ($10^{-20.699}$ to 10^{-17} m²), and thus,*
24 *assigning this material as anhydrite MB in the model has essentially the same effect as*
25 *calling it concrete, as long as pressures are below the fracture initiation pressure.*
- 26 *2. In the case of high pressures, it is expected that fracturing may occur in the anhydrite*
27 *MBs and flow could go “around” the panel closures out of the two-dimensional plane*
28 *considered in the model grid. In this case, the flow would be through the MB material,*
29 *which incorporates a fracture model, as described above.*

30 *PA-4.2.8.3 Disturbed Rock Zone Above the Panel Closure*

31 *After construction of the concrete portion of the panel closure, the salt surrounding the*
32 *monolith will be subjected to compressive stresses, which will facilitate the rapid healing of*
33 *disturbed halite. The rounded configuration of the monolith creates a situation very favorable*
34 *for concrete durability: high compressive stresses and low stress differences. In turn, the*
35 *compressive stresses developed within the salt will quickly heal any damage caused by*
36 *construction excavation, thereby eliminating the DRZ along the length of this portion of the*

1 *panel closure. The permeability of the salt immediately above and below the rigid concrete*
2 *monolith component of Option D will approach the intrinsic permeability of the undisturbed*
3 *Salado halite.*

4 *To represent the DRZ above the monoliths, the CRA-2004 PA uses the material, DRZ_PCS, in*
5 *the BRAGFLO grid (Figure PA-8). The values assigned to DRZ_PCS are the same as those*
6 *values used for the DRZ above the excavated areas (material DRZ_1, see Table PA-2), except*
7 *for the properties PRMX_LOG, PRMY_LOG, and PRMZ_LOG, the logarithm of permeability*
8 *in the x, y, and z directions, respectively. These permeability values are assigned the same*
9 *distributions used for the material CONC_PCS. In this instance, the values are based on the*
10 *nature of the model set-up, and not directly on experimental data (although the general range*
11 *of the distribution agrees with experimental observations of healed salt). The use of these*
12 *permeabilities ensures that any fluid flow is equally probable through or around the Option D*
13 *panel closures and represents the range of uncertainty that exists in the performance of the*
14 *panel closure system.*

15 *PA-4.2.8.4 Empty Drift and Explosion Wall Materials*

16 *The DRF_PCS is the material representing the empty drift and explosion wall. For simplicity,*
17 *this material is assumed to have hydrologic properties equivalent to the material representing*
18 *the waste panel and is used for the three sets of panel closures represented in the grid (Figure*
19 *PA-8). The creep closure model is applied to this material to be consistent with the*
20 *neighboring materials. The assignment of a high permeability to this region containing the*
21 *explosion wall is justified because the explosion wall is not designed to withstand the stresses*
22 *imposed by creep closure and will be highly permeable following rapid room closure.*

23 *PA-4.2.9 Borehole Model*

24 *The major disruptive event in the CRA-2004 PA is the penetration of the repository by a*
25 *drilling intrusion. In the undisturbed scenario (scenario S1; see Section PA-6.7.1), these*
26 *blocks have the material properties of the neighboring stratigraphic or excavated modeling*
27 *unit, and there is no designation in the grid of a borehole except for the reduced lateral*
28 *dimensions of this particular column of grid blocks.*

29 *In the scenarios simulating drilling disturbance, these cells start out with the same material*
30 *properties as in the undisturbed scenario, but at the time of intrusion the borehole grid blocks*
31 *are reassigned to borehole material properties. The drilling intrusion is modeled by modifying*
32 *the permeability of the grid blocks in column 26 of Figure PA-8 (values listed in Table PA-5).*
33 *Further, the drilling intrusion is assumed to produce a borehole with a diameter of 12.25 in.*
34 *(0.31 m) (Vaughn 1996; Howard 1996); borehole fill is assumed to be incompressible;*
35 *capillary effects are ignored; residual gas and brine saturations are set to zero; and porosity is*
36 *set to 0.32 (see materials CONC_PLG, BH_OPEN, BH_SAND and BH_CREEP in Table*
37 *PA-2). When a borehole that penetrates pressurized brine in the Castile Formation is*
38 *simulated (i.e., an E1 intrusion), the permeability modifications indicated in Table PA-5*
39 *extend from the land surface (i.e., grid cell 2155 in Figure PA-10) to the base of the*
40 *pressurized brine (i.e., grid cell 2225 in Figure PA-10). When a borehole that does not*
41 *penetrate pressurized brine in the Castile Formation is under consideration (i.e., an E2*

1 intrusion), the permeability modifications indicated in Table PA-5 stop at the bottom of the
 2 lower DRZ (i.e., grid cell 1111 in Figure PA-10).

3 **Table PA-5. Permeabilities for Drilling Intrusions Through the Repository**

<i>Time After Intrusion</i>	<i>Assigned Permeabilities</i>
0 - 200 years	Concrete plugs are assumed to be emplaced at the Santa Rosa Formation (i.e., a surface plug with a length of 15.76 m; corresponds to grid cells 2113, 2155 in Figure PA-10) and the Los Medanós Member of the Rustler Formation (i.e., a plug at top of Salado with a length of 36 m; corresponds to grid cell 1644 in Figure PA-10). Concrete plugs are assumed to have a permeability of $k = 5 \times 10^{-17} \text{ m}^2$; open portions of the borehole are assumed to have a permeability of $1 \times 10^{-9} \text{ m}^2$. See material CONC_PLG in Table PA-3.
200 - 1200 years	Concrete plugs are assumed to fail after 200 years (DOE 1995) an entire borehole is assigned a permeability typical of silty sand, i.e., $k = 10^x \text{ m}^2$, $x = \text{BHPRM}$, where BHPRM is an uncertain input to the analysis (see Table PA-17). See material BH_SAND in Table PA-3.
> 1200 years	Permeability reduced by one order of magnitude in Salado Formation beneath repository due to creep closure of borehole (Thompson et al. 1996) (i.e., $k = 10^x/10$, $x = \text{BHPRM}$, in grid cells 2225, 1576, 26, 94, 162, 230, 1111, 1119, 1127 of Figure PA-10). No changes are made within and above the lower DRZ. See material BH_CREEP in Table PA-3.

4 **PA-4.2.10 Numerical Solution**

5 Determination of gas and brine flow in the vicinity of the repository requires the numerical
 6 solution of the two nonlinear partial differential equations in Equation (42) on the
 7 computational domain in Figure PA-8 together with evaluation of appropriate auxiliary
 8 conditions (Equation (25f), Equation (25g), and Equation (41)). The actual unknown
 9 functions in this solution are p_b and S_g , although the constraint conditions also give rise to
 10 values for p_g and S_b . As two dimensions in space and one dimension in time are in use, p_b , p_g ,
 11 S_b and S_g are functions of the form $p_b(x, y, t)$, $p_g(x, y, t)$, $S_b(x, y, t)$ and $S_g(x, y, t)$.

12 The solution of Equation (42) requires both initial value and boundary value conditions for p_b
 13 and S_g . The initial value conditions for p_b and S_g are given in Section PA.4.2.2. As indicated
 14 there, the calculation starts at time $t = -5$ years, with a possible resetting of values at $t = 0$
 15 years, which corresponds to final waste emplacement and sealing of the repository. The
 16 boundary conditions are such that no brine or gas moves across the exterior grid boundary
 17 (Table PA-6). This Neumann-type boundary condition is maintained for all time. Further,
 18 BRAGFLO allows the user to specify pressure and/or saturation at any grid block. This
 19 feature is used to specify Dirichlet-type conditions at the surface grid blocks
 20 ($i = 1, 2, \dots, 68, j = 33$, Figure PA-8) and at the far field locations in the Culebra and Magenta
 21 Formations ($i = 1, 68, j = 26$ and $i = 1, 68, j = 28$, Figure PA-8). These auxiliary conditions
 22 are summarized in Table PA-7).

1 **Table PA-6. Boundary Value Conditions for p_g and p_b**

Boundaries below ($y = 0$ m) and above ($y = 1039$ m) system for $0 \leq x \leq 46630$ m and -5 yr $\leq t$	
$\left(\nabla p_g + \rho_g g \nabla h\right)\Big _{(x,y,t)} \cdot j = 0$ Pa / m	<i>no gas flow condition</i>
$\left(\nabla p_b + \rho_b g \nabla h\right)\Big _{(x,y,t)} \cdot j = 0$ Pa / m	<i>no brine flow condition</i>
Boundaries at left ($x = 0$ m) and right ($x = 46630$ m) of system for $0 \leq y \leq 1039$ m and -5 yr $\leq t$	
$\left(\nabla p_g + \rho_g g \nabla h\right)\Big _{(x,y,t)} \cdot i = 0$ Pa / m	<i>no gas flow condition</i>
$\left(\nabla p_b + \rho_b g \nabla h\right)\Big _{(x,y,t)} \cdot i = 0$ Pa / m	<i>no brine flow condition</i>

2 **Table PA-7. Auxiliary Dirichlet Conditions for p_b and S_g**

Surface Grid Blocks	
$S_g(i, j, t) = 0.08363$	$i = 1, 2, \dots, 68, j = 33, -5$ yr $\leq t$
$p_b(i, j, t) = 1.01 \times 10^5$ Pa	$i = 1, 2, \dots, 68, j = 33, -5$ yr $\leq t$
Culebra and Magenta Far Field	
$p_b(i, 26, t) = 8.22 \times 10^5$ Pa	$i = 1$ and $68, j = 26, -5$ yr $\leq t$ (Culebra)
$p_b(i, 28, t) = 9.17 \times 10^5$ Pa	$i = 1$ and $68, j = 28, -5$ yr $\leq t$ (Magenta)

3 *A fully implicit finite difference procedure is used to solve Equation (42). The associated*
 4 *discretization of the gas mass balance equation is given by*

$$\begin{aligned}
 & \frac{1}{\Delta x_i} \left\{ \frac{1}{x_{i+1} - x_i} \left[\frac{\alpha \rho_g k_x k_{rg}}{\mu_g} \right]_{i+1/2, j}^{n+1} \left(\Phi_{g_{i+1, j}}^{x-} - \Phi_{g_{i, j}}^{x+} \right)^{n+1} \right. \\
 & \quad \left. - \frac{1}{x_i - x_{i-1}} \left[\frac{\alpha \rho_g k_x k_{rg}}{\mu_g} \right]_{i-1/2, j}^{n+1} \left(\Phi_{g_{i, j}}^{x-} - \Phi_{g_{i-1, j}}^{x+} \right)^{n+1} \right\} \\
 & \quad + \frac{1}{\Delta y_j} \left\{ \frac{1}{y_{j+1} - y_j} \left[\frac{\alpha \rho_g k_y k_{rg}}{\mu_g} \right]_{i, j+1/2}^{n+1} \left(\Phi_{g_{i, j+1}}^{y-} - \Phi_{g_{i, j}}^{y+} \right)^{n+1} \right.
 \end{aligned}$$

$$\begin{aligned}
 & \left. -\frac{1}{y_j - y_{j-1}} \left[\frac{\alpha \rho_g k_y k_{rg}}{\mu_g} \right]_{i,j-1/2}^{n+1} \left(\Phi_{g,i,j}^{y-} - \Phi_{g,i,j-1}^{y+} \right)^{n+1} \right\} \\
 & + \alpha_{i,j} q_{wg,i,j}^{n+1} + \alpha_{i,j} q_{rg,i,j}^{n+1} - \frac{\left(\alpha \phi \rho_g S_g \right)_{i,j}^{n+1} - \left(\alpha \phi \rho_g S_g \right)_{i,j}^n}{\Delta t} = 0, \tag{79}
 \end{aligned}$$

where Φ represents the phase potentials given by

$$\Phi_{g,i,j}^{x+} = p_{g,i,j} + \rho_{g,i+1/2,j} g h_{i,j}, \quad \Phi_{g,i,j}^{x-} = p_{g,i,j} + \rho_{g,i-1/2,j} g h_{i,j}$$

and

$$\Phi_{g,i,j}^{y+} = p_{g,i,j} + \rho_{g,i,j+1/2} g h_{i,j}, \quad \Phi_{g,i,j}^{y-} = p_{g,i,j} + \rho_{g,i,j-1/2} g h_{i,j},$$

and the subscripts are defined by

i = x-direction grid index

j = y-direction grid index

$i \pm 1/2$ = x-direction grid block interface

$j \pm 1/2$ = y-direction grid block interface

x_i = grid block center in the x-coordinate direction (m)

y_j = grid block center in the y-coordinate direction (m)

Δx_i = grid block length in the x-coordinate direction (m)

Δy_j = grid block length in the y-coordinate direction (m),

the superscripts are defined by

n = index in the time discretization, known solution time level

$n+1$ = index in the time discretization, unknown solution time level,

and the interblock densities are defined by

$$\rho_{g,i+1/2,j} = \frac{\Delta x_{i+1,j}}{\Delta x_{i,j} + \Delta x_{i+1,j}} \rho_{g,i,j} + \frac{\Delta x_{i,j}}{\Delta x_{i,j} + \Delta x_{i+1,j}} \rho_{g,i+1,j},$$

$$\rho_{gi-1/2,j} = \frac{\Delta x_{i,j}}{\Delta x_{i-1,j} + \Delta x_{i,j}} \rho_{g,i-1,j} + \frac{\Delta x_{i-1,j}}{\Delta x_{i-1,j} + \Delta x_{i,j}} \rho_{gi,j},$$

$$\rho_{gi,j+1/2} = \frac{\Delta y_{i,j+1}}{\Delta y_{i,j} + \Delta y_{i,j+1}} \rho_{gi,j} + \frac{\Delta y_{i,j}}{\Delta y_{i,j} + \Delta y_{i,j+1}} \rho_{gi,j+1},$$

$$\rho_{gi,j-1/2} = \frac{\Delta y_{i,j}}{\Delta y_{i,j-1} + \Delta y_{i,j}} \rho_{gi,j-1} + \frac{\Delta y_{i,j-1}}{\Delta y_{i,j-1} + \Delta y_{i,j}} \rho_{gi,j}.$$

The interface values of k_{rg} in Equation (79) are evaluated using upstream weighted values (i.e., the relative permeabilities at each grid block interface are defined to be the relative permeabilities at the center of the adjacent grid block that has the highest potential). Further, interface values for $\alpha \rho_g k_x / \mu_g$ and $\alpha \rho_g k_y / \mu_g$ are obtained by harmonic averaging of adjacent grid block values for these expressions.

The discretization of the brine mass balance equation is obtained by replacing the subscript for gas, g , by the subscript for brine, b . As a reminder, p_g and S_b are replaced in the numerical implementation with the substitutions indicated by Equation (25d) and Equation (25c), respectively. For the CRA-2004 PA, wells are not used in the conceptual model. Thus, the terms q_{wg} and q_{wb} are zero. For this analysis, the wellbore is not treated by a well model, but rather is explicitly modeled within the grid as a distinct material region (i.e., Upper Borehole and Lower Borehole in Figure PA-8).

The resultant coupled system of nonlinear brine and gas mass balance equations is integrated in time using the Newton-Raphson method with upstream weighting of the relative permeabilities as previously indicated. The primary unknowns at each computational cell center are brine pressure and gas saturation.

PA-4.2.11 Gas and Brine Flow across Specified Boundaries

The Darcy velocity vectors $\mathbf{v}_g(x, y, t)$ and $\mathbf{v}_b(x, y, t)$ for gas and brine flow ($(m^3/m^2)/s = m/s$) are defined by the expressions

$$\mathbf{v}_g(x, y, t) = \mathbf{K}_g k_{rg} (\nabla p_g + \rho_g \mathbf{g} \nabla h) / \mu_g \quad (80)$$

and

$$\mathbf{v}_b(x, y, t) = \mathbf{K}_b k_{rb} (\nabla p_b + \rho_b \mathbf{g} \nabla h) / \mu_b. \quad (81)$$

Values for \mathbf{v}_g and \mathbf{v}_b are obtained and saved as the numerical solution of Equation (42) is carried out. Cumulative flows of gas, $C_g(t, \mathcal{B})$, and brine, $C_b(t, \mathcal{B})$, from time 0 to time t across an arbitrary boundary \mathcal{B} in the domain of (Figure PA-8) is then given by

$$C_l(t, \mathcal{B}) = \int_0^t \left[\int_{\mathcal{B}} \alpha(x, y) \mathbf{v}_l(x, y, t) \cdot \mathbf{n}(x, y) ds \right] dt \quad (82)$$

for $l = g, b$, where $\alpha(x, y)$ is the geometry factor defined in Figure PA-9, $\mathbf{n}(x, y)$ is an outward pointing unit normal vector, and $\int_{\mathcal{B}} ds$ denotes a line integral. As an example, \mathcal{B} could correspond to the boundary of the waste disposal regions in Figure PA-8. The integrals defining $C_g(t, \mathcal{B})$ and $C_b(t, \mathcal{B})$ are evaluated using the Darcy velocities defined by Equation (80) and Equation (81). Due to the dependence of gas volume on pressure, $C_g(t, \mathcal{B})$ is typically calculated in moles or in m^3 at standard temperature and pressure, which requires an appropriate change of units for \mathbf{v}_g in Equation (82).

PA-4.2.12 Additional Information

Additional information on BRAGFLO and its use in the CRA-2004 PA can be found in the BRAGFLO User's Manual (WIPP PA 2003c) and in the analysis package for the Salado flow calculations for the CRA-2004 PA (Stein and Zelinski 2003b).

PA-4.3 Radionuclide Transport in the Salado: NUTS

This section describes the model used to compute transport of radionuclides in the Salado for E0, E1 and E2 scenarios (defined in Section 6.3). The model for transport in the E1E2 scenario is described in Section PA-4.4.

PA-4.3.1 Mathematical Description

The following system of partial differential equations is used to model radionuclide transport in the Salado:

$$-\nabla \cdot \alpha \mathbf{v}_b C_{bl} + \alpha S_l = \alpha \frac{\partial}{\partial t} (\phi S_b C_{bl}) + (\alpha \phi S_b C_{bl}) \lambda_l - \alpha \phi S_b \sum_{p \in P(l)} C_{bp} \lambda_p \quad (83a)$$

$$-S_l = \frac{\partial}{\partial t} (C_{sl}) + C_{sl} \lambda_l - \sum_{p \in P(l)} C_{sp} \lambda_p \quad (83b)$$

for $l = 1, 2, \dots, nR$, where

\mathbf{v}_b = Darcy velocity vector ($(m^3/m^2)/s = m/s$) for brine (supplied by BRAGFLO from solution of Equation (81)),

C_{bl} = concentration (kg/m^3) of radionuclide l in brine,

1 C_{sl} = concentration (kg/m³) of radionuclide l in solid phase (i.e., not in brine), with
 2 concentration defined with respect to total (i.e., bulk) formation volume (only
 3 used in repository; see Figure PA-8),

4 S_l = linkage term ((kg/m³)/s) due to dissolution/precipitation between
 5 radionuclide l in brine and in solid phase (see Equation (84)),

6 ϕ = porosity (supplied by BRAGFLO from solution of Equation (25)),

7 S_b = brine saturation (supplied by BRAGFLO from solution of Equations (25)),

8 λ_l = decay constant (s⁻¹) for radionuclide l ,

9 $P(l)$ = { p : radionuclide p is a parent of radionuclide l },

10 nR = number of radionuclides,

11 and α is the dimension dependent geometry factor in Equation (26). The CRA-2004 PA uses a
 12 two-dimensional representation for fluid flow and radionuclide transport in the vicinity of the
 13 repository with α defined by the element depths in Figure PA-8. Although omitted from the
 14 notation for brevity, the terms α , \mathbf{v}_b , C_{bb} , C_{sb} , S_b , ϕ and S_b are functions $\alpha(x, y)$, $\mathbf{v}_b(x, y, t)$,
 15 $C_{bl}(x, y, t)$, $C_{sl}(x, y, t)$, $S_l(x, y, t)$, $\phi(x, y, t)$, and $S_b(x, y, t)$ of time t and the spatial
 16 variables x, y . Equation (83) is defined and solved on the same computational grid used with
 17 BRAGFLO for the solution of Equation (25) (Figure PA-8).

18 Radionuclides are assumed to be present in both brine (Equation (83a)) and in an immobile
 19 solid phase (Equation (83b)). Radionuclide transport takes place only by brine flow (Equation
 20 (83a)). A maximum radionuclide concentration in brine is assumed for each element (Section
 21 PA-4.3.2). Then, each individual radionuclide equilibrates between the brine and solid phases
 22 on the basis of the maximum concentration of its associated element and the mole fractions of
 23 other isotopes of this element that are included in the calculation. The linkage between the
 24 brine and solid phases in Equation (83) accomplished by the term S_b , where

$$S_l = \begin{cases} \delta(\tau - t) \text{Dif}(S_T, C_{b,El(l)}) MF_{sl} & \text{if } 0 \leq \text{Dif}(S_T, C_{b,El(l)}) \leq C_{s,El(l)} / (\phi S_b), 0 < S_b \\ \delta(\tau - t) [C_{s,El(l)} / (\phi S_b)] MF_{sl} & \text{if } 0 \leq C_{s,El(l)} / (\phi S_b) < \text{Dif}(S_T, C_{b,El(l)}), 0 < S_b, (84) \\ \delta(\tau - t) \text{Dif}(S_T, C_{b,El(l)}) MF_{bl} & \text{if } \text{Dif}(S_T, C_{b,El(l)}) < 0, 0 < S_b \\ 0 & \text{otherwise} \end{cases}$$

26 with

1 $S_T [Br(t), Ox(l), Mi, El(l)] =$ maximum concentration (kg/m³) of element $El(l)$ in
 2 oxidation state $Ox(l)$ in brine type $Br(t)$, where $El(l)$ denotes the element
 3 of which radionuclide l is an isotope, $Ox(l)$ denotes the oxidation state in
 4 which element $El(l)$ is present, Mi indicates whether microbial activity is
 5 present, and $Br(t)$ denotes the type of brine present in the repository at time
 6 t (see Section PA-4.3.2 for definition of $S_T(Br, Ox, Mi, El)$).

7 $C_{p,El(l)} =$ concentration (kg/m³) of element $El(l)$ in brine ($p = b$) or solid ($p = s$) (i.e.,
 8 sum of concentrations of radionuclides that are isotopes of same element as
 9 radionuclide l , where $k \in El(l)$ only if k is an isotope of element $El(l)$)
 10
$$= \sum_{k \in El(l)} C_{pk} \tag{85}$$

11 $Dif(S_T, C_{b,El(l)}) =$ difference (kg/m³) between maximum concentration of element $El(l)$ in
 12 brine and existing concentration of element $El(l)$ in brine
 13
$$= S_T [Br(t), Ox(l), Mi, El(l)] - C_{b,El(l)} \tag{86}$$

14 $MF_{pl} =$ mole fraction of radionuclide l in phase p , where $p = b \sim$ brine and
 15 $p = s \sim$ solids
 16
$$= C_{pl} CM_l / \sum_{k \in El(l)} C_{pk} CM_k \tag{87}$$

17 $CM_l =$ conversion factor (mole/kg) from kilograms to moles for radionuclide l

18 $\delta(\tau - t) =$ Dirac delta function (s⁻¹) (i.e., $\delta(\tau - t) = 0$ if $\tau \neq t$ and $\int_{-\infty}^{\infty} \delta(\tau - t) d\tau = 1$).

19 Although omitted for brevity, the terms S_b , $C_{p,El(l)}$, MF_{pl} , ϕ and S_b are functions of time t
 20 and spatial variables x, y . The Dirac delta function, $\delta(t - \tau)$, appears in Equation (84) to
 21 indicate that the adjustments to concentration are implemented instantaneously within the
 22 numerical solution of Equation (83) whenever a concentration imbalance is observed.

23 The velocity vector \mathbf{v}_b in Equation (83) is defined in Equation (81) and is obtained from the
 24 numerical solution of Equation (25). If \mathcal{B} denotes an arbitrary boundary (e.g., the land
 25 withdrawal boundary) in the domain of Equation (83) (i.e., Figure PA-8), then the cumulative
 26 transport of $C_l(t, \mathcal{B})$ of radionuclide l from time 0 to time t across \mathcal{B} is given by

$$C_I(t, \mathcal{B}) = \int_0^t \left[\int_{\mathcal{B}} \mathbf{v}_b(x, y, t) C_I(x, y, t) \alpha(x, y) \cdot \mathbf{n}(x, y) ds \right] dt, \quad (88)$$

where $\mathbf{n}(x, y)$ is an outward pointing unit normal vector and $\int_{\mathcal{B}} ds$ denotes a line integral over \mathcal{B} .

Equation (83) models advective radionuclide transport due to the velocity vector \mathbf{v}_b . Although the effects of solubility limits are considered, no chemical or physical retardation is included in the model. Also, molecular diffusion is not included in the model, with this omission having little effect as the radionuclides under consideration have molecular diffusion coefficients on the order of 10^{-10} m²/s and thus can be expected to move approximately 10 m over 10,000 years due to molecular diffusion. Mechanical dispersion is also not included, with this omission having little effect on the final results due to the uniform initial radionuclide concentrations assumed within the repository and the use of time-integrated releases in assessing compliance with 40 CFR § 191.13.

PA-4.3.2 Calculation of Maximum Concentration $S_T(\text{Br}, \text{Ox}, \text{Mi}, \text{El})$

A maximum concentration $S_T(\text{Br}, \text{Ox}, \text{Mi}, \text{El})$ (mol/l) is calculated for each brine type (Br ~ Salado, Castile), oxidation state (Ox ~ +3, +4, +5, +6), presence of microbial action (present or not) and element (El ~ Am, Pu, U, and Th). The maximum concentration is given by

$$S_T(\text{Br}, \text{Ox}, \text{Mi}, \text{El}) = S_D(\text{Br}, \text{Ox}, \text{Mi}, \text{El}) + S_C(\text{Br}, \text{Ox}, \text{Mi}, \text{El}), \quad (89)$$

where $S_D(\text{Br}, \text{Ox}, \text{Mi}, \text{El})$ is the dissolved solubility (mol/l) and $S_C(\text{Br}, \text{Ox}, \text{Mi}, \text{El})$ is the concentration (mol/l) of the element sorbed to colloids.

The dissolved solubility $S_D(\text{Br}, \text{Ox}, \text{Mi}, \text{El})$ is given by

$$S_D(\text{Br}, \text{Ox}, \text{Mi}, \text{El}) = S_{FMT}(\text{Br}, \text{Ox}, \text{Mi}) \times 10^{UF(\text{Br}, \text{Ox}, \text{El})} \quad (90)$$

where

$S_{FMT}(\text{Br}, \text{Ox}, \text{Mi})$ = dissolved solubility (mol/l) calculated by FMT model (WIPP PA 1998a) for brine type Br, oxidation state Ox, and presence of microbial action Mi,

$UF(\text{Br}, \text{Ox}, \text{El})$ = logarithm (base 10) of uncertainty factor for solubilities calculated by FMT expressed as a function of brine type Br, oxidation state Ox and element El.

Table PA-8 lists the calculated values of $S_{FMT}(\text{Br}, \text{Ox}, \text{Mi})$; details of the calculation are provided in Attachment SOTERM. The values of Mi are determined by the uncertain

1 *parameter WMICDFLG; see Table PA-17. The uncertainty factors $UF(Br, Ox, El)$ are*
 2 *determined by the uncertain parameters listed in Table PA-9; definition of each uncertain*
 3 *parameter is provided in Table PA-17.*

4 **Table PA-8. Calculated Values for Dissolved Solubility**

<i>Brine/Microbial action</i>	<i>Oxidation State</i>			
	<i>+3</i>	<i>+4</i>	<i>+5</i>	<i>+6</i>
<i>Salado/No microbial gas generation</i>	3.07×10^{-7}	1.24×10^{-8}	9.72×10^{-7}	8.7×10^{-6}
<i>Castile/No microbial gas generation</i>	1.77×10^{-7}	5.84×10^{-9}	2.13×10^{-5}	8.8×10^{-6}
<i>Salado/With microbial gas generation</i>	3.07×10^{-7}	1.19×10^{-8}	1.02×10^{-6}	8.7×10^{-6}
<i>Castile/With microbial gas generation</i>	1.69×10^{-7}	2.47×10^{-8}	5.08×10^{-6}	8.8×10^{-6}

5 **Table PA-9. Uncertainty Factors for Dissolved Solubility**

<i>Brine</i>	<i>Oxidation State, Element</i>					
	<i>+3, Am</i>	<i>+3, Pu</i>	<i>+4, Pu</i>	<i>+4, U</i>	<i>+6, U</i>	<i>+4, Th</i>
<i>Salado</i>	<i>WSOLAM3S</i>	<i>WSOLPU3S</i>	<i>WSOLPU4S</i>	<i>WSOLU4S</i>	<i>WSOLU6S</i>	<i>WSOLTH4S</i>
<i>Castile</i>	<i>WSOLAM3C</i>	<i>WSOLPU3C</i>	<i>WSOLPU4C</i>	<i>WSOLU4C</i>	<i>WSOLU6C</i>	<i>WSOLTH4C</i>

6 *The concentration (mol/l) of the element sorbed to colloids $S_C(Br, Ox, Mi, El)$ is given by*

7
$$S_C(Br, Ox, Mi, El) = S_{Hum}(Br, Ox, Mi, El) + S_{Mic}(Br, Ox, Mi, El) + S_{Act}(El) + S_{Mn}, \quad (91)$$

8 *where*

9 $S_{Hum}(Br, Ox, Mi, El)$ = *solubility (i.e., concentration expressed in mol/l) in brine type Br of*
 10 *element El in oxidation state Ox with or without microbial action (Mi)*
 11 *resulting from formation of humic colloids*

12
$$= \min \{ SF_{Hum}(Br, Ox, El) \times S_D(Br, Ox, Mi, El), UB_{Hum} \}$$

13 $SF_{Hum}(Br, Ox, El)$ = *scale factor used as a multiplier on $S_D(Br, Ox, Mi, El)$ in definition*
 14 *of $S_{Hum}(Br, Ox, Mi, El)$ (see Table PA-10),*

1 **Table PA-10. Scale Factor $SF_{Hum}(Br, Ox, El)$ Used in Definition of $S_{Hum}(Br, Ox, Mi, El)$**

Brine	Oxidation state, Element					
	+3, Am	+3, Pu	+4, Pu	+4, U	+6, U	+4, Th
Salado	0.19	0.19	6.3	6.3	0.12	6.3
Castile	WPHUMOX3 ¹	WPHUMOX3 ¹	6.3	6.3	0.51	6.3

¹ See Table PA-17.

2 UB_{Hum} = upper bound on solubility (i.e., concentration expressed in mol/l) of
 3 individual actinide elements resulting from formation of humic colloids
 4 = 1.1×10^{-5} mol/l,

5 $S_{Mic}(Br, Ox, Mi, El)$ = solubility (i.e., concentration expressed in mol/l) in brine type Br of
 6 element El in oxidation state Ox with or without microbial action (Mi)
 7 resulting from formation of microbial colloids
 8 = $\min\{SF_{Mic}(Ox, Mi, El) \times S_D(Br, Ox, Mi, El), UB_{Mic}(Ox, El)\}$,

9 $SF_{Mic}(Ox, Mi, El)$ = scale factor used as multiplier on $S_D(Br, Ox, Mi, El)$ in definition of
 10 $S_{Mic}(Br, Ox, Mi, El)$ (see Table PA-11),

11 $UB_{Mic}(Ox, El)$ = upper bound on solubility (i.e., concentration expressed in mol/l) of element
 12 El in oxidation state Ox resulting from formation of microbial colloids (see
 13 Table PA-11),

14 **Table PA-11. Scale Factor $SF_{Mic}(Ox, Mi, El)$ and Upper Bound $UB_{Mic}(Ox, Mi, El)$ (mol/l)**
 15 **Used in Definition of $S_{Mic}(Br, Ox, Mi, El)$**

	Oxidation state, Element					
	+3, Am	+3, Pu	+4, Pu	+4, U	+6, U	+4, Th
No Microbial Action						
$SF_{Mic}(Ox, Mi, El)$	0.0	0.0	0.0	0.0	0.0	0.0
$UB_{Mic}(Ox, Mi, El)$	0.0	0.0	0.0	0.0	0.0	0.0
Microbial Action						
$SF_{Mic}(Ox, Mi, El)$	3.6	0.3	0.3	2.1×10^{-3}	2.1×10^{-3}	3.1
$UB_{Mic}(Ox, Mi, El)$	1	6.8×10^{-5}	6.8×10^{-5}	2.1×10^{-3}	2.1×10^{-3}	1.9×10^{-3}

$$S_{Act}(El) = \text{solubility (i.e., concentration expressed in mol/l) of element El resulting from formation of actinide intrinsic colloids}$$

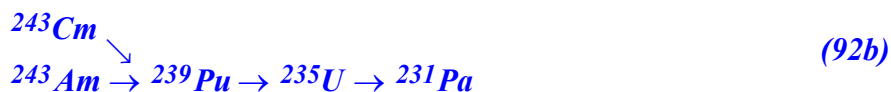
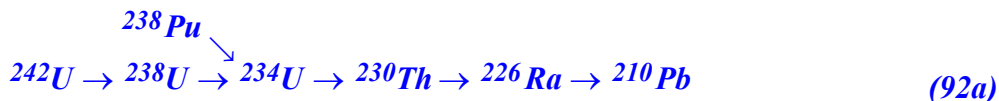
$$= \begin{cases} 1 \times 10^{-9} \text{ mol/l} & \text{if El = plutonium} \\ 0 & \text{mol/l otherwise} \end{cases},$$

$$S_{Mn} = \text{solubility (i.e., concentration expressed in mol/l) of individual actinide element resulting from formation of mineral fragment colloids}$$

$$= 2.6 \times 10^{-8} \text{ mol/l.}$$

PA-4.3.3 Radionuclides Transported

Appendix TRU WASTE (Table TRU WASTE-9) lists the radionuclides included in the transport calculations. With the exceptions of ¹³⁷Cs, ¹⁴⁷Pm, and ⁹⁰Sr, the radionuclides in Table TRU WASTE-9 belong to the following decay chains:



Since the solution of Equation (83) for this many radionuclides and decay chains would be very time-consuming, the number of radionuclides for direct inclusion in the analysis was reduced using the algorithm shown in Appendix TRU WASTE (Figure TRU WASTE-5); the rationale for each radionuclide excluded from transport is presented in Table TRU WASTE-10. The CRA-2004 PA uses the same reduction algorithm as was used in the CCA PA (see CCA Appendix WCA); the algorithm was found to be acceptable in the review of the CCA (EPA 1998, Section 4.6.1.1).

After the reduction of radionuclides summarized in Table TRU WASTE-10, the following 10 radionuclides remained from the decay chains shown above:



1 *Next, ²³⁸Pu was eliminated from transport calculations due to its short half-life (87.8 years).*
 2 *The remaining nine radionuclides were then further reduced by combining radionuclides that*
 3 *have similar decay and transport properties. In particular, ²³⁴U, ²³⁰Th, and ²³⁹Pu were used*
 4 *as surrogates for the groups {²³⁴U, ²³³U}, {²³⁰Th, ²²⁹Th}, and {²⁴²Pu, ²³⁹Pu, ²⁴⁰Pu}, with the*
 5 *initial inventories of ²³⁴U, ²³⁰Th and ²³⁹Pu being redefined to account for the additional*
 6 *radionuclide(s) in each group. In redefining the initial inventories, the individual*
 7 *radionuclides were combined on either a mole or curie basis (i.e., moles added and then*
 8 *converted back to curies or curies added directly). In each case, the method that maximized*
 9 *the combined inventory was used, i.e.: ²³³U was added to ²³⁴U by curies; ²⁴⁰Pu was added to*
 10 *²³⁹Pu by curies; ²⁴²Pu was added to ²³⁹Pu by moles; and ²²⁹Th was added to ²³⁰Th by curies.*
 11 *In addition, ²⁴¹Pu was added to ²⁴¹Am by moles because ²⁴¹Pu has a half life of 14 years and*
 12 *will quickly decay to ²⁴¹Am, and neglect of this ingrowth would underestimate the ²⁴¹Am*
 13 *inventory by about four percent (Table PA-12). The outcome of this process was the following*
 14 *five radionuclides and three simplified decay chains:*

15
$$^{241}\text{Am}, \ ^{238}\text{Pu} \rightarrow \ ^{234}\text{U} \rightarrow \ ^{230}\text{Th}, \ ^{239}\text{Pu}, \quad (94)$$

16 *which were then used with Equation (83) for transport in the vicinity of the repository and*
 17 *also for transport in the Culebra Dolomite (Section PA-4.9). These radionuclides account for*
 18 *99 percent of the EPA units in the waste after 2,000 years (Appendix TRU WASTE, Table*
 19 *TRU WASTE-9), and hence will dominate any releases by transport.*

20 *Table PA-12. Combination of Radionuclides for Transport*

<i>Combination</i>	<i>Isotope Initial Values</i>	<i>Combination Procedure</i>	<i>Combined Inventory</i>
<i>²³³U → ²³⁴U</i>	<i>1.27 × 10³ Ci ²³³U 3.19 × 10² Ci ²³⁴U</i>	<i>1.27 × 10³ Ci ²³³U → 1.27 × 10³ Ci ²³⁴U</i>	<i>1.59 × 10³ Ci ²³⁴U</i>
<i>²⁴²Pu → ²³⁹Pu ²⁴⁰Pu → ²³⁹Pu</i>	<i>2.71 × 10¹ Ci ²⁴²Pu 1.08 × 10⁵ Ci ²⁴⁰Pu 6.65 × 10⁵ Ci ²³⁹Pu</i>	<i>2.71 × 10¹ Ci ²⁴²Pu = 2.82 × 10¹ moles ²⁴²Pu → 2.82 × 10¹ moles ²³⁹Pu = 4.24 × 10² Ci ²³⁹Pu 1.08 × 10⁵ Ci ²⁴⁰Pu → 1.08 × 10⁵ Ci ²³⁹Pu</i>	<i>7.73 × 10⁵ Ci ²³⁹Pu</i>
<i>²²⁹Th → ²³⁰Th</i>	<i>5.39 × 10⁰ Ci ²²⁹Th 1.76 × 10⁻¹ Ci ²³⁰Th</i>	<i>5.39 × 10⁰ Ci ²²⁹Th → 5.39 × 10⁰ Ci ²³⁰Th</i>	<i>5.57 × 10⁰ Ci ²³⁰Th</i>
<i>²⁴¹Pu → ²⁴¹Am</i>	<i>5.38 × 10⁵ Ci ²⁴¹Pu 4.58 × 10⁵ Ci ²⁴¹Am</i>	<i>5.38 × 10⁵ Ci ²⁴¹Pu = 2.15 × 10¹ moles ²⁴¹Pu → 2.15 × 10¹ moles ²⁴¹Am = 1.80 × 10⁴ Ci ²⁴¹Am</i>	<i>4.60 × 10⁵ Ci ²⁴¹Am</i>